

# Haloes, molecules and multineutrons<sup>†</sup>

F. Miguel MARQUÉS MORENO

*Laboratoire de Physique Corpusculaire,  
IN2P3-CNRS, ENSICAEN et Université de Caen, F-14050 Caen cedex, France*

**Abstract:** Away from the equilibrium between protons and neutrons within stable nuclei, many exotic nuclei exist. Most of the known nuclear properties evolve smoothly with exoticism, but some extreme proton-neutron combinations have revealed during the last decade completely new concepts. They will be illustrated through three examples: the extended and dilute halo formed by very weakly bound neutrons, the molecular-like neutron orbitals found in nuclei exhibiting  $\alpha$  clustering, and the recently revived debate on the possible existence of neutral nuclei. The different experimental results will be reviewed, and we will see how several properties of these new phenomena can be well understood within relatively simple theoretical approaches.

**Resumé:** Loin de l'équilibre entre protons et neutrons dans les noyaux stables, existent beaucoup de noyaux exotiques. La plupart des propriétés nucléaires connues évoluent doucement avec l'exotisme, mais certaines combinaisons proton-neutron nous ont révélé pendant la dernière décennie des concepts complètement nouveaux. Ils seront illustrés à travers trois exemples : le halo étendu et diffus formé par des neutrons très faiblement liés, les orbitales neutron de type moléculaire qui apparaissent dans des noyaux formés d'agrégats  $\alpha$ , et le débat récemment relancé sur la possible existence de noyaux neutres. Nous passerons en revue les différents résultats expérimentaux, et nous verrons comment certaines propriétés de ces nouveaux phénomènes peuvent être comprises à travers des approches théoriques relativement simples.

---

<sup>†</sup> Lecture presented at "École Joliot-Curie de Physique Nucléaire", Maubuisson (France), Sep. 8–14 2002.

## Contents

<b>1</b>	<b>Introduction</b>	<b>2</b>	3.2	The nuclear concepts . . . . .	17
1.1	Beyond nuclear drops . . . . .	2	3.3	Deformed harmonic oscillator . . . . .	18
<b>2</b>	<b>Halo nuclei</b>	<b>3</b>	3.4	More complex molecules . . . . .	21
2.1	An expected effect? . . . . .	4	<b>4</b>	<b>Multineutrons</b>	<b>22</b>
2.2	The configuration of the cloud . . . . .	5	4.1	For and (mostly) against . . . . .	22
2.3	Theoretical models . . . . .	9	4.2	The quest: 1960s-2000s . . . . .	25
2.4	Beyond two neutrons . . . . .	12	4.3	A new approach . . . . .	26
<b>3</b>	<b>Nuclear molecules</b>	<b>14</b>	4.4	The near future . . . . .	27
3.1	True molecules . . . . .	14	<b>5</b>	<b>Summary</b>	<b>28</b>

# 1 Introduction

The force between nucleons remains unknown, at least qualitatively, after more than seventy years of research, and only quantitative phenomenological fits are available since the 1990s [1]. These fits are not strictly derived from QCD and contain more than 50 parameters, but describe well the world data base on  $pp$  and  $np$  scattering. However, already when attempting to model the very lightest nuclei,  ${}^3\text{H}$  and  ${}^3,4\text{He}$ , an entirely phenomenological three-body force (no  $NNN$  data are available) needs to be added. Indeed, the complexity of nuclear forces is reflected in the huge variety of nuclei that can be formed with only protons and neutrons.

It is therefore surprising that a model like the liquid drop, with only five parameters, provides an overall good description (within few MeV) of the g.s. energy of most known nuclei. The binding energy of a nucleus,  $Nm_n + Zm_p - M(N, Z)$ , is given by:

$$B(N, Z) = a_v A - a_s A^{2/3} - a_c \frac{Z^2}{A^{1/3}} - a_a \frac{(N-Z)^2}{A} \pm \frac{\delta}{A^{1/2}} \quad (1)$$

The first three terms are justified by some nuclear properties analog to liquid drops: constant density and saturation (volume term), surface tension (surface term), and electrical repulsion between protons (Coulomb term). The other two terms are added in order to mimic some quantum properties: the Pauli principle favours configurations where  $N \approx Z$ , which fill the neutron and proton potential wells up to a similar energy (asymmetry term), and protons and neutrons couple to form pairs (pairing term) [2].

Even if we know that the nucleus is much more complex, the simplicity of Eq. (1) leads us to imagine nuclei as liquid drops. We believe them to have:

- **sharp** limits ( $R \approx r_0 A^{1/3}$ );
- **uniform** volume ( $\rho[r] \approx \rho_0$ );
- **homogeneous**  $p$ - $n$  mixture ( $\rho_n \approx \frac{N}{Z} \rho_p$ ).

Eq. (1) can be extended to take into account other effects, like deformation, shell closures, Wigner term... but all of them are compatible with the liquid drop picture. The fact that many exotic nuclei, with  $N/Z$  ratios different from those of the stable isotopes, have been studied in the past decades was neither in contradiction with this picture, as their lower binding was just accounted for by the asymmetry term in Eq. (1) or more sophisticated versions (Sec. 4).

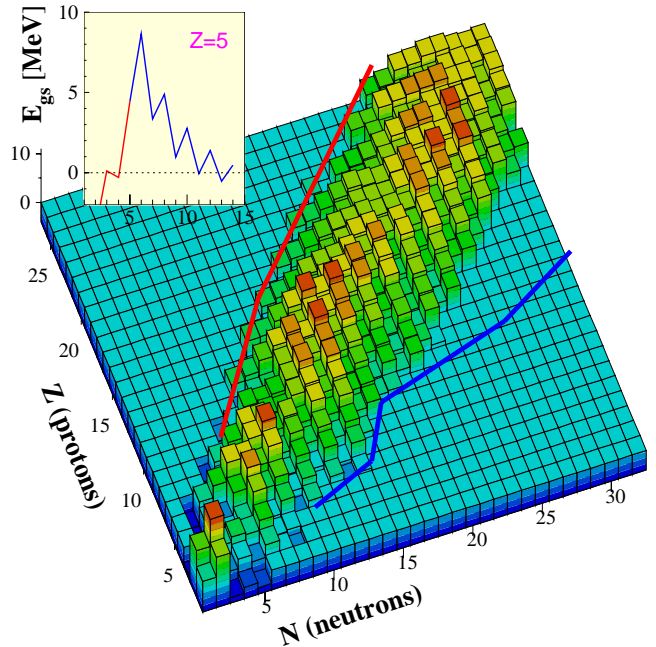


Figure 1: The ridge of stability.  $E_{\text{gs}}(N, Z)$  is defined as the minimum mass difference between the nucleus and a partition of  $N$  neutrons and  $Z$  protons — the binding energy with respect to the first particle threshold. The red and blue lines correspond to the proton and neutron drip lines, and the insert to the boron isotopes.

## 1.1 Beyond nuclear drops

However, among the huge number of exotic nuclei already discovered, few have been recently found to exhibit new properties that do not correspond to a drop at all:

- The typical example are **halo nuclei** (Sec. 2), in which the weakly bound valence neutrons violate the three characteristics listed above — sharpness, uniformity and homogeneity — forming a low-density distribution extending far beyond the core of the nucleus.
- Another example are **nuclear molecules** (Sec. 3), neutron-rich nuclei exhibiting properties analog to covalent binding in atomic molecules. In these systems,  $\alpha$  particles play the role of atomic nuclei and the valence neutrons act like molecular electrons: the exchange of these nucleons between the  $\alpha$  clusters provides additional stability and effectively binds the “ $\alpha$  chains”.
- The possible existence of a third kind of nuclei, which would resemble a drop but with a very

unusual composition, will be finally addressed (Sec. 4): **neutron drops**; or multineutrons, or neutron clusters, or neutral nuclei... lots of names for a still hypothetical object!

All these systems are light, neutron-rich nuclei. There are two reasons for this (Fig. 1). They are neutron-rich because the Coulomb barrier confines protons, even weakly bound, in the nucleus, and prevents the existence of  $N/Z \ll 1$  nuclei. Really extreme  $N/Z$  configurations have thus to be searched for on the neutron-rich side, but the most neutron-rich isotopes have only been created for light nuclei.

When having a look to the “beginning” of the nuclear chart (Fig. 2) the leading role of clustering in the landscape becomes clear. All three subjects of this course are indeed connected by the same idea: how **clustering** manifests, and correlations between clusters act, in specific configurations of protons and neutrons. Therefore, by studying these nuclei we will not only learn about their own properties, but also about the way the nuclear force forms clusters inside nuclei and leads to residual forces between them.

The nature of these residual forces is at the basis of problems as fundamental as the nucleosynthesis of carbon — and all nuclei beyond. As sketched in Fig. 2, the ending of the primordial nucleosynthesis is due to the inability of these forces to bind binary systems, like  ${}^5\text{He}$ ,  ${}^5\text{Li}$  or  ${}^8\text{Be}$ . Only the appearance of three-body correlations between clusters enables the continuation of the process through nuclei like  ${}^6\text{He}$ ,  ${}^9\text{Be}$  or  ${}^{12}\text{C}$ , and thereon the nucleosynthesis of heavier nuclei.

Details about the production of beams of exotic nuclei can be found in [3, Y. Blummenfeld]. The results that will illustrate this course have been mostly obtained with exotic beams produced by in-flight fragmentation of a primary beam. Concerning the detectors, most of the experiments will face the detection of neutrons, one of the most elusive particles. Theoretically, we will see how existing models have been extended and new ones have been created, and how simple approaches provide, at first order, the description of many of these new nuclear properties.

## 2 Halo nuclei

By adding/subtracting neutrons successively to a stable nucleus, the chain of isotopes reaches the neutron/proton drip line, where the binding energy of the last nucleon(s) approaches zero (inset in Fig. 1). On the neutron drip line, these weakly bound nuc-

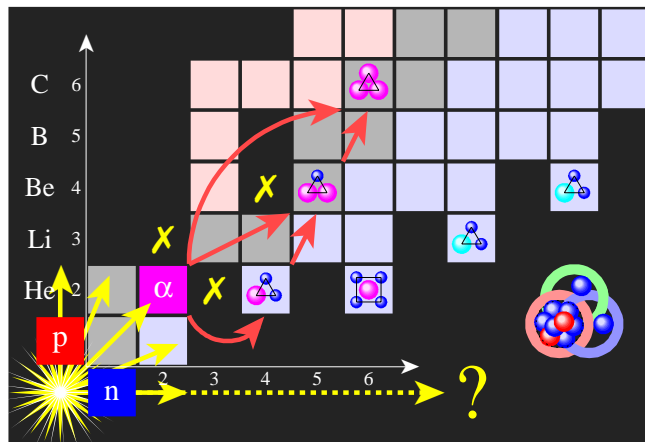


Figure 2: The Segré chart for light nuclei. The well established many-neutron haloes,  ${}^6,8\text{He}$ ,  ${}^{11}\text{Li}$  and  ${}^{14}\text{Be}$ , are indicated on the neutron drip line. The arrows show the different paths towards carbon, all involving three-body systems ( ${}^6\text{He}$ ,  ${}^9\text{Be}$  and  ${}^{12}\text{C}^*$ ). The sketch on the right represents the Borromean binding of the three clusters in  ${}^{14}\text{Be}$ , and the dashed arrow the location of hypothetical neutral nuclei on the chart.

leons may form a low-density veil around the other (core) nucleons. We talk about halo neutrons around a “normal” central nucleus, like the sketch of  ${}^{14}\text{Be}$  in Fig. 2. How far/close is this picture from reality?

In an atom, the nucleons move within several fm, and the electrons beyond several thousands of fm. The distribution of very weakly bound neutrons can extend to several tens of fm. Therefore, even with a halo the nucleus is still a negligible point inside the atom. However, at the nuclear level an order of magnitude is a **huge effect**, and a huge theoretical challenge, as the wave function of a halo nucleon has to be calculated in a box of  $\sim 10^6 \text{ fm}^3$ !

If we now want to think about the nucleus as an ensemble of nucleons, and not of probability distributions, we need to “freeze” the position of the neutrons. A relevant picture is given by the rms separations, between the halo neutrons and between their c.m. and the core nucleus (Fig. 3). Not only, on average, the three bodies do not overlap, but the separations are much bigger than the ranges of the corresponding binary interactions. The system has a large probability (often more than 50%) of being in classically forbidden configurations, and thus a sketch like the one shown in Fig. 2 for  ${}^{14}\text{Be}$  is not exaggerated at all.

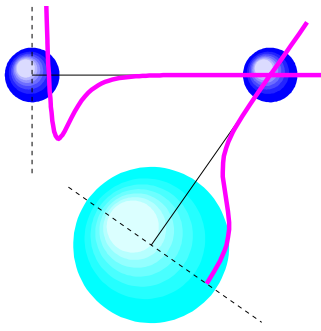


Figure 3: Average (rms) separation of  ${}^9\text{Li}$  and the halo neutrons in  ${}^{11}\text{Li}$ , as obtained from a three-body calculation [4]. The range of the binary interactions is indicated.

## 2.1 An expected effect?

But, is there something strange behind the halo? No. We all know from elementary quantum mechanics that, as the binding energy of a particle in a potential well goes to zero, its probability distribution spreads more and more outside the well. The strange thing about the halo is that this indeed *does* happen in “real life” nuclei.

The simplest case is a neutron (no Coulomb barrier) with  $\ell = 0$  (no centrifugal barrier) bound at an energy  $E = -\varepsilon$  in a square well of depth  $V_0$  and radius  $R$ . The Schrödinger equation leads then to an analytical wave function:

$$r \psi(r) \propto \begin{cases} \sin(kr) & , r < R \\ \sin(kR) e^{-\alpha(r-R)} & , r > R \end{cases} \quad (2)$$

where  $k = \sqrt{2\mu(V_0 - \varepsilon)}$  and  $\alpha = \sqrt{2\mu\varepsilon}$ . Outside the well the wave function vanishes exponentially: the smaller the binding energy  $\varepsilon$  (and then  $\alpha$ ), the further the veil extends.

We can get a quantitative idea of the effect, for example for a neutron in a square well corresponding to a nucleus of  $A = 10$  ( $R = 2.6$  fm), by increasing the depth  $V_0$  starting from 0. Below 8 MeV there are no bound states. Then a bound state appears, and it gets more and more strongly bound as we keep increasing  $V_0$ . When going beyond 75 MeV a second bound state appears, just at the top of the well. The corresponding density distributions for these two states are shown in Fig. 4. The first state has a very small probability of being outside the well (6%), but the second one is most of the time (85%) outside.

Obviously  $\lim_{\varepsilon \rightarrow 0} P(r > R) = 1$ . The analytical dependence of  $P(r > R)$  with  $\varepsilon$  can be extracted from

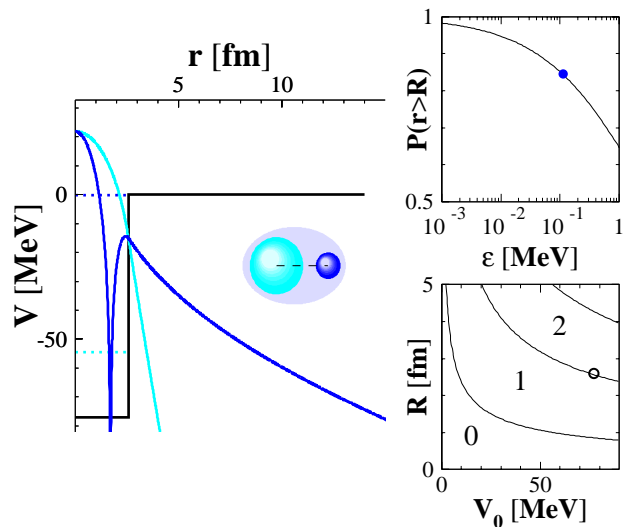


Figure 4: Density distributions,  $|\psi(r)|^2$  [Eq. (2)], in logarithmic scale for the two bound states in a well of  $V_0 = 77$  MeV and  $R = 2.6$  fm. The right panels represent: the probability of being outside the well as a function of the binding energy  $\varepsilon$  ( $\bullet$  is the second state); and the regions corresponding to 0, 1 and 2 bound states as a function of the depth and radius of the well ( $\circ$  are the values used).

Eq. (2), and is plotted in Fig. 4. This is not *strictly* true, as for a given  $V_0$  and  $R$  there are only discrete solutions for  $\varepsilon$  (the closed symbol), but illustrates well the potentially huge extent of the halo effect for extremely weak binding. The whole range of  $\varepsilon$  can be mapped by varying  $V_0$  and/or  $R$  (Fig. 4). The lines correspond to the limits for having  $N$  bound states:  $R = \pi(N - \frac{1}{2})\hbar c / \sqrt{2\mu V_0}$  [5, p. 244]. Within each region, the new state becomes more deeply bound when approaching the next line.

But there is a “real”, well-known example: the **deuteron**, where the neutron is bound to the proton by  $\varepsilon = 2.2$  MeV. Its wave function has long been known, and Eq. (2) provides a solution very close to that obtained with much more complex potentials [5, p. 125]. The probability for the neutron being at  $r > R$ , even if the binding energy is still few MeV, is as big as 66%. This is thus the first halo nucleus, with a halo as big as the core!

In 1985, experiments lead by Tanihata at Berkeley with exotic beams of about 800 MeV/N revealed interaction cross-sections significantly higher for few very neutron-rich isotopes [6]. The interaction probability can be roughly linked to the size of a nucleus by:

$$\sigma_I \propto \pi (R + R_{\text{target}})^2 \quad (3)$$

It was clearly a threshold effect, as even for the other neutron-rich isotopes radii increased smoothly as expected for a liquid drop [Fig. 10(a)]. The **abnormal sizes** correspond to haloes of one neutron ( $^{11}\text{Be}$ ,  $S_n = 0.5$  MeV), two ( $^6\text{He}$ ,  $^{11}\text{Li}$ ,  $^{14}\text{Be}$ ,  $S_{2n} = 1.0, 0.3, 1.3$  MeV) and four ( $^8\text{He}$ ,  $S_{4n} = 3.1$  MeV). Having a look to Fig. 4 the halo hypothesis [7] seems now straightforward, but it took few years to settle down before other experiments confirmed that the protons were not participating to this increase [8, 9].

Further reanalysis of the cross-sections, taking into account the few-body structure of these nuclei [10], has lead to even higher radii for  $^6\text{He}$  (2.7 fm) and  $^{11}\text{Li}$  (3.5 fm). For  $^{11}\text{Li}$  it corresponds to the radius of  $^{48}\text{Ca}$ . But we have seen that halo nuclei are not uniform objects, if they were the density of  $^{11}\text{Li}$  would be  $1/4$  of  $\rho_0$ ! Halo nuclei have two distinct phases, the dense heavy core and the diffuse light halo (Fig. 4), and so a single size measure cannot provide the true extent of the halo. Following theoretical calculations, the size of the halo alone in  $^{11}\text{Li}$  corresponds to about 6 fm: two nucleons occupy the same volume than 208 in Pb!

Another novel property of halo nuclei is related to the Heisenberg's uncertainty principle. The halo neutrons move in a volume much bigger than the core nucleus, and thus their momentum content is much lower, they “**move slower**” than nucleons in all nuclei we knew. This property was confirmed and exploited in breakup experiments, in which narrow momentum distributions for the neutrons and/or the core nucleus were measured [11].

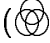
We will not go into further details concerning one-neutron haloes. Their structure can be already understood with calculations as simple as the square well described above; even for more complex potentials, the asymptotic wave function (there where  $V \approx 0$ ) is given by Eq. (2). The theoretical efforts concentrate now on the description of reactions involving these nuclei (see [3, Y. Blumenfeld]). The case of  $^8\text{He}$ , with  $\alpha$ - $4n$  structure, will be discussed in Sec. 4. In the following we will concentrate on two-neutron haloes.

## 2.2 The configuration of the cloud

Two-neutron halo nuclei can be considered as core- $n$ - $n$  systems. When two neutrons form the halo, there are properties much more intriguing than “just” a size effect:

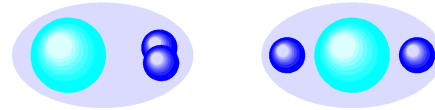
- The  $N$ - $N$  interaction could be studied up to now, either free, either at  $\rho \sim \rho_0$ . Different

densities are obtained during heavy-ion collisions, but just ephemerally. In g.s. halo nuclei we find, for the first time, nucleons at  $\rho \ll \rho_0$ .

- The odd-even staggering in the binding energy (Fig. 1) leads, close to the drip line, to a series of unbound-bound systems. In two-neutron haloes, the core- $n$  system is unbound, as the  $n$ - $n$  is. A three-body system in which the removal of *any* body breaks it up is known as Borromean, by analogy to the Borromean rings [4] (, Fig. 2).

Therefore, the binding of these nuclei is a pure three-body effect. As such, they represent a unique route towards the understanding of **three-body correlations**, which are, for example, responsible for the  $3\alpha$  process described above, and essential nowadays in all ab initio calculations of light nuclei [12].

The first theoretical descriptions of two-neutron haloes were reduced to a two-body problem, as the one in Fig. 4, by considering a dineutron cluster around the core [7]. However, the configuration of the three-body system can be as different as:



Indeed, theoretical calculations predict the coexistence of both [4], named *dineutron* and *cigar* configurations, respectively. How can we probe them?

Measurements like interaction cross-sections or momentum content of the fragments are sensitive to the overall size, detailed correlation effects being integrated out. Knowing how the neutrons distribute themselves around the core requires second generation, more subtle experiments. The lower cross-sections force these experiments to be run only on  $^6\text{He}$ , the two-neutron halo closest to stability.

### Two-neutron transfer

Intuitively, the probability of transferring the two halo neutrons to a target nucleus should be linked to the importance of the dineutron configuration. Details on transfer reactions as a probe of the structure of halo nuclei can be found in [3, Y. Blumenfeld]. Here we will just note the  $^6\text{He} + ^4\text{He}$  elastic scattering results at Dubna [13]. The data are shown in Fig. 5.

The forward angles are easily described by the elastic scattering of  $^6\text{He}$  on the  $^4\text{He}$  target. The increase at backward angles is due to transfer of the

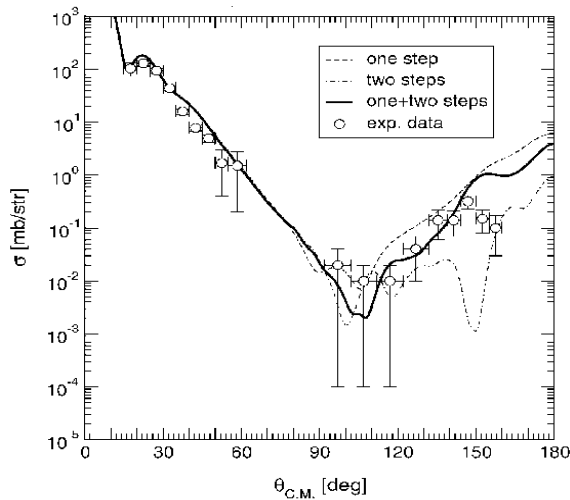


Figure 5:  ${}^6\text{He} + {}^4\text{He}$  elastic scattering at 151 MeV [13]. Calculations correspond to elastic scattering with two-step (sequential) and/or one-step (direct) transfer contributions [14].

two halo neutrons from the projectile to the target:

$$\sigma(\theta) \propto |A_{\text{elastic}}(\theta) + A_{2n}(\pi - \theta)|^2 \quad (4)$$

The data were first analysed [13] assuming the contribution of *only* one-step direct reaction mechanisms. Consequently, the part of the wave function corresponding to the dineutron configuration was found to contribute the most to  $2n$  transfer, and these results were presented as a probe of the dineutron configuration in  ${}^6\text{He}$ .

More complete calculations [14] suggest, however, that this connection between  $2n$  transfer and dineutron configuration is not as straightforward as expected (Fig. 5). The inclusion of two-step processes and indirect routes via the  $2^+$  excited state in  ${}^6\text{He}$ , within the framework of coupled reaction channels, indicates that “*the sequential process may be still of importance, implying that the dineutron structure is an effective description*” of the reaction [14]. From this reference, it seems that details of the reaction **dynamics** lead the  $2n$  transfer more than details of the wave function itself.

## Radiative capture

An investigation of coherent bremsstrahlung production in the reaction  $\alpha(p, \gamma)$  at 50 MeV demonstrated that the high-energy photon spectrum is dominated by capture to form  ${}^5\text{Li}$  [15]. Such results motivated the extension of this technique to study  ${}^6\text{He}$ . Given a proton wavelength of  $\lambda = 0.7$  fm at 40 MeV, it

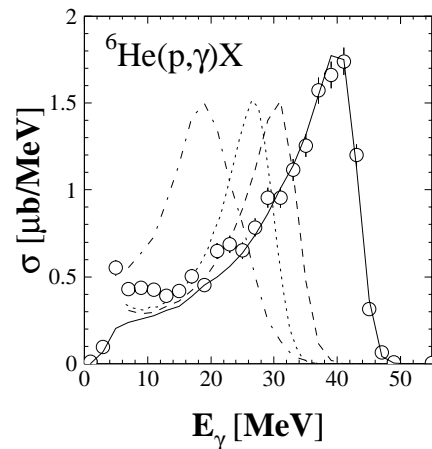


Figure 6: Energy distribution, in the  ${}^6\text{He}+p$  c.m., for photons in coincidence with  ${}^7\text{Li}$ . The lines (arbitrarily normalized) correspond to the response of the array to  $E_\gamma = 42$  MeV (solid) and to calculations of quasi-free proton capture on the  ${}^5\text{He}$  cluster (dashed), the  $\alpha$  core (dotted) and one halo neutron (dotted-dashed), respectively [16].

should be possible to observe direct capture, as a quasi-free process, on the constituents of  ${}^6\text{He}$  in addition to capture into  ${}^7\text{Li}$ . Moreover, capture on the different clusters would lead to different  $E_\gamma$  in the range 20–40 MeV.

The experiment was run at GANIL with a 40 MeV/N  ${}^6\text{He}$  beam, a solid hydrogen target, the SPEG spectrometer for the detection of the charged reaction products, and the “Château de Cristal” array (74 BaF<sub>2</sub> crystals placed around the target covering  $\Omega \sim 70\%$ ) for the detection of high-energy photons [16]. Capture into  ${}^7\text{Li}$  was observed as the strongest channel (Fig. 6): the photon energy spectrum corresponds to a  $\gamma$ -ray line at 42 MeV.

There were also coincidences between  $\gamma$ -rays and fragments lighter than  ${}^7\text{Li}$ , and the corresponding energy spectra did exhibit peaks below 42 MeV [16]. They were well described by calculations (Fig. 6) of quasi-free capture on a halo neutron (into  $d$ ), the  $\alpha$  core (into  ${}^5\text{Li}$ ) and  ${}^5\text{He}$  (into  ${}^6\text{Li}_{0+}^*$ , the  $T = 1$  analogue of  ${}^6\text{He}$  [17]). Importantly, the capture events on the  $\alpha$  core corresponded well to the ones observed for the free  $\alpha(p, \gamma)$  reaction [15] taking into account the intrinsic momentum of the  $\alpha$  particle in  ${}^6\text{He}$ .

Nonetheless, two quasi-free capture processes were not observed:  $2n(p, \gamma)t$  and  $t(p, \gamma)\alpha$  [16]. This is simply explained by the absence of capture on the  $\alpha$ - $2n$  [4] and  $t$ - $t$  [18] configurations, respectively, and suggests that the dominant configuration for the  ${}^6\text{He}$

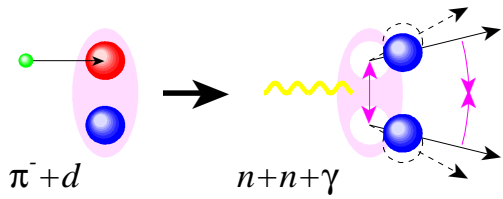


Figure 7: Schematic view of the reaction  $\pi^- d \rightarrow (nn)\gamma$ . In the absence of  $n$ - $n$  interaction, the photon and the neutrons (dashed lines) share the energy following phase space. The attractive interaction gets neutron velocities (solid arrows) closer, depending on the intensity of the attraction and the  $n$ - $n$  distance.

g.s. is  $\alpha$ - $n$ - $n$  in which the  $n$ - $n$  separation is relatively large [16]. If this was the case, lower energy protons should be able to form tritons and probe larger distance correlations between the neutrons.

## Interferometry

The previous experiments relied on very low cross-sections, and were thus limited to  ${}^6\text{He}$ . There is, however, a powerful technique sensitive to the relative configuration of two neutrons that can be applied to the high cross-section breakup channel: two-neutron *interferometry*. Therefore, it can be extended to the more exotic two-neutron haloes  ${}^{11}\text{Li}$  and  ${}^{14}\text{Be}$ , and soon to  ${}^{17}\text{B}$ .

In the absence of final state interactions,  $A$  particles in the final state of a reaction would share the available energy following the kinematics of  $A$ -body phase space [19]. Any interaction between particles will modify this phase-space sharing, depending on: (i) the **nature** of the interaction; and (ii) the **distance** between particles. If we are able to calculate/extract the phase-space contribution, and we study a particle pair for which the interaction is known, then we can measure the relative distance\*.

A clear example is the reaction  $\pi^- d \rightarrow (nn)\gamma$  (Fig. 7), which is used to study the  $n$ - $n$  interaction (Sec. 4). The cross-section as a function of the  $n$ - $n$  relative momentum  $q$  can be written as:

$$\sigma(q) \approx \sigma_0(q) \times \left| \int \psi_d \psi_s^*(a_{nn}) d^3r \right|^2 \quad (5)$$

where the phase space distribution  $\sigma_0(q)$  is modulated by the overlap integral, over the relative dis-

\*An analog argument leads, in  $\alpha$  decay, to a relation between the final energy of the  $\alpha$  particle, the  $\alpha$ -nucleus Coulomb interaction, and the distance at which the  $\alpha$  particle left the nucleus.

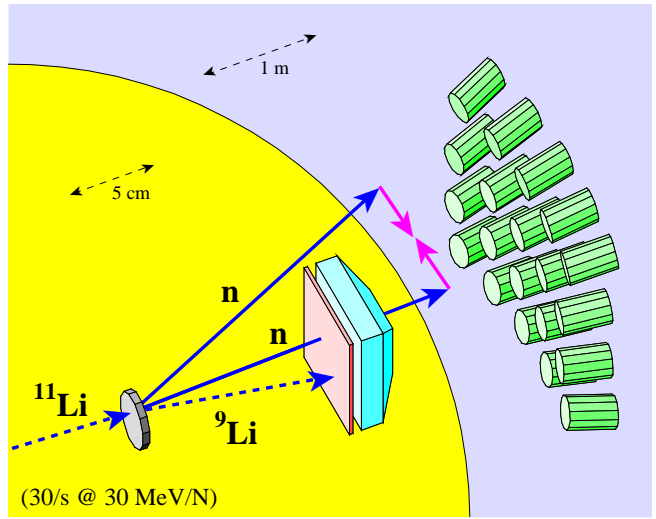


Figure 8: Setup of the neutron interferometry experiment [21]: inside the chamber, the Si-CsI telescope forward of the target; outside, the closest wall of 20 neutron detectors — four walls and 90 detectors were used.

tance, between the initial deuteron and the final  $n$ - $n$  wave functions [20]. The former contains the relative distance between the two nucleons — well-known in the deuteron — and the latter contains the  $n$ - $n$  interaction, characterized by the  $n$ - $n$  scattering length  $a_{nn}$  [Eq. (40)] — which can be thus determined.

We can therefore apply the same argument, using the known  $a_{nn}$ , to a system in which the relative distance between neutrons is unknown. In the case of the breakup of a two-neutron halo, the neutron relative momentum distribution can, by analogy to Eq. (5), be written as:

$$\sigma(q) \approx \sigma_0(q) \times \left| \int \psi_{\text{halo}}(r) \psi_s^* d^3r \right|^2 \quad (6)$$

This technique was applied to the breakup of  ${}^6\text{He}$ ,  ${}^{11}\text{Li}$  and  ${}^{14}\text{Be}$  beams (30–50 MeV/N) on Pb and C targets at GANIL [21]. Part of the setup is sketched in Fig. 8. The array of 90 neutron detectors, DEMON, was placed at forward angles in a staggered arrangement of four walls in order to minimize and reject any contribution from neutron cross-talk [22].

The first element of Eq. (6), the measured  $\sigma(q)$ , is shown in Fig. 9(a) for the breakup of  ${}^{11}\text{Li}$ . The whole distribution is at low relative momenta because halo neutrons themselves have low momenta. The second element, the uncorrelated or phase-space contribution  $\sigma_0(q)$ , is obtained by mixing neutrons from different events [21]. A crucial point for applying this more or less standard technique to halo neutrons is

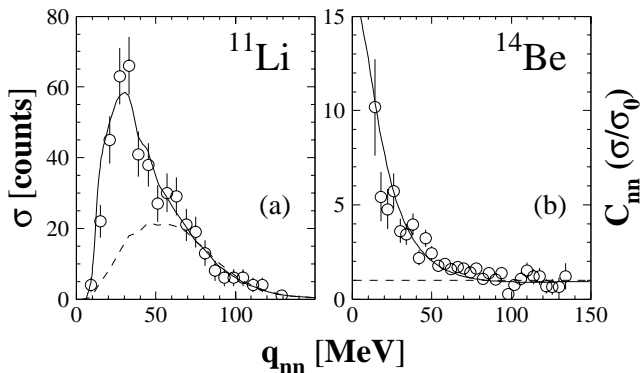


Figure 9: Neutron relative momentum distributions for the  $^{11}\text{Li} \rightarrow (nn)^9\text{Li}$  and  $^{14}\text{Be} \rightarrow (nn)^{12}\text{Be}$  breakup on Pb [21]: (a) symbols are the data, the dashed line the uncorrelated distribution obtained by event mixing, and the solid line the effect of the  $n$ - $n$  interaction for  $r_{nn}^{\text{rms}} = 6.6$  fm; (b) symbols are the ratio of the measured and uncorrelated distributions, and the solid line the effect of the  $n$ - $n$  interaction for  $r_{nn}^{\text{rms}} = 5.6$  fm.

the removal of residual correlations through an iterative technique, which will not be described here — for details see [21, 23]. The result is the dashed line in Fig. 9(a).

The ratio  $\sigma/\sigma_0$  provides the interference term in Eq. (6), commonly known as *correlation function* [24], which can be expressed here as:

$$C_{nn}(q) = \frac{\sigma}{\sigma_0} \approx \left| \int \psi_{\text{halo}}(r) \psi_s^* d^3r \right|^2 \quad (7)$$

The correlation function is shown in Fig. 9(b) for the breakup of  $^{14}\text{Be}$ . The attractive  $n$ - $n$  interaction manifests itself through an increase of the relative momentum distributions at low values.

The interference term was interpreted following the formalism of [25] and assuming a Gaussian relative distance distribution for the halo neutrons (solid lines in Fig. 9). The fact that the single neutron distributions in halo nuclei do not correspond to Gaussians is not important, as the relative distributions are not very sensitive to the shape of the single ones. Yukawa-like or uniform-sphere single particle distributions, provided they correspond to the same  $r_n^{\text{rms}}$ , lead to relative distributions close to the Gaussian one [26].

The distances extracted for the three systems,  $r_{nn}^{\text{rms}} \sim 6$  fm [Fig. 10(b)], are of the order of twice the one expected between independent nucleons within a sphere of  $R = r_0 A^{1/3}$  (dashed line) and even bigger than the — already big —  $n$ - $p$  distance in the

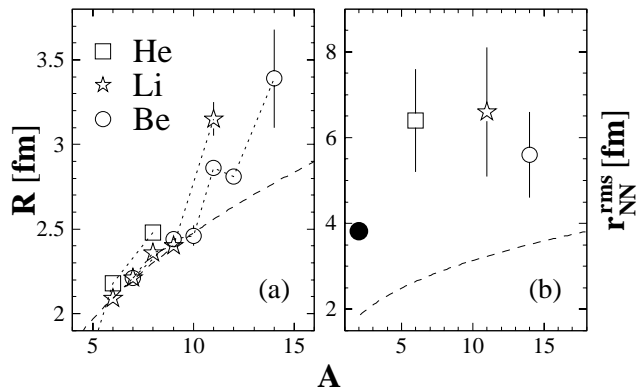


Figure 10: (a) Interaction radii deduced from reaction cross-sections of neutron-rich He, Li and Be isotopes [6]; (b) average  $n$ - $n$  distances deduced from interferometry analyses [21, 27], compared to the  $n$ - $p$  distance in the deuteron. The dashed lines represent the expectation for a uniform sphere of radius  $r_0 A^{1/3}$  (a) and the corresponding average  $N$ - $N$  distance (b).

deuteron. These results are in agreement with the conclusions drawn from the radiative capture experiment on  $^6\text{He}$ : the two halo neutrons would be, on average, far away from each other.

### Three-body correlations

In the preceding discussion the problem was reduced to the spatial  $n$ - $n$  distance. But Eq. (7) can be extended to four dimensions: the correlation function is then studied over the relative momentum *and* energy, and depends on the  $n$ - $n$  distance *and* the delay between the emission of the two neutrons [25]. The correlation function becomes not only a femtometer, but also a **clock**!

The moderate statistics (Fig. 9) do not allow for the unfolding of space and time distances, but the delay of a neutron in a three-particle system necessarily means that it formed a resonance with the remaining core nucleus with a finite lifetime. Therefore, standard techniques used in particle physics for the study of correlations in three-particle systems, such as Dalitz plot analyses [28], can be applied here to map the evolution of the final state.

The Dalitz plots for the  $^{14}\text{Be} \rightarrow (nn)^{12}\text{Be}$  breakup on Pb and C targets are shown in Fig. 11, as a function of the normalized  $n$ - $n$  and core- $n$  invariant masses [27]. A system of non-interacting particles corresponds to a uniform population of the plot. Clearly, in the case of Coulomb-dominated breakup (a) the  $n$ - $n$  interaction accounts well for the



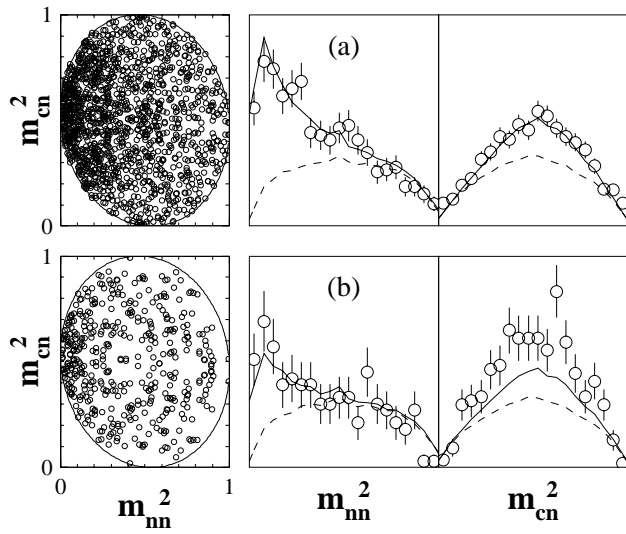


Figure 11: Dalitz plots (core- $n$  vs  $n$ - $n$ ), and the projections onto both axes, for the  $^{14}\text{Be} \rightarrow (nn)^{12}\text{Be}$  breakup on Pb (a) and C (b) targets. The lines are the result of a phase space simulation (dashed), plus the  $n$ - $n$  interaction for  $r_{nn}^{\text{rms}} = 5.6, 7.6$  fm respectively (solid).

strong departure from uniformity observed, and suggests that no  $^{13}\text{Be}$  resonances are being significantly formed: the  $r_{nn}^{\text{rms}}$  measured corresponds thus to the  $n$ - $n$  separation in the halo of  $^{14}\text{Be}$ .

For nuclear breakup (b) two facts are evident: the  $n$ - $n$  signal is weaker, and this interaction alone does not describe the distributions so well. This suggests the formation of resonances in  $^{13}\text{Be}$ , which is confirmed in the  $^{12}\text{Be}+n$  energy spectrum [27]. The delay needed to explain the decrease from Pb to C target of the  $n$ - $n$  signal corresponds to  $150_{-150}^{+250}$  fm/ $c$ , or  $(5_{-5}^{+8}) 10^{-22}$  s, and can be attributed to the average lifetime of the resonances formed [27].

### 2.3 Theoretical models

Mean-field approximations of the many-body problem succeed in describing properties of heavy nuclei, in which each nucleon “sees” the mean field created by all the others. When nuclei become lighter, the  $N$ - $N$  interaction plays an increasing role, and mean-field models are extended by considering pairing correlations [3, H. Flocard]. These approaches are no longer valid when nuclei develop a halo, because the mean field of the halo neutrons differs from that of the core nucleons: the halo is too dilute and contains too few nucleons to allow a mean-field description.

In general, any kind of correlations beyond pairing, as all **clustering phenomena** (Fig. 2), need to be

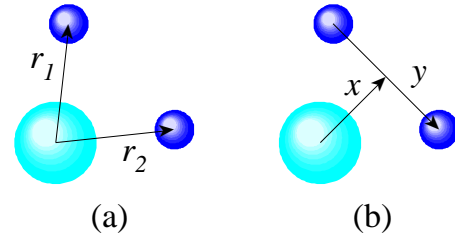


Figure 12: Relative coordinates used in core- $n$ - $n$  models: (a) between each neutron and the core; (b) between neutrons and between the core and their c.m. — Jacobi coordinates.

included “by hand”. The details of the many-body system are then ignored, and special attention is paid to few-body correlations between clusters (considered inert or with some simple excitation structure). Of course, some observables will be out of reach for these models, but we have seen that the existence of halo nuclei is due to a delicate balance between the cluster correlations near threshold. Therefore, they should reproduce the more relevant properties of these systems.

### The two-neutron subspace

These clustering phenomena appear close to few-body thresholds of the system. The core+ $n$ + $n$  threshold is the one closest to the g.s., and none of the two-body systems are bound. Therefore, a description in terms of these three bodies is the natural one for general, low-energy properties, of the  $A$  nucleon system. The wave function of the nucleus is written as a product of the core and the two-neutron wave functions,  $\Psi(A) = \Psi_c \Psi_{2n}$ . The core is considered inert, and thus the *active* part of the wave function is  $\Psi_{2n}$ . We are left with a two-neutron problem [29]:

$$(\mathbf{H}_{cn_1} + \mathbf{H}_{cn_2} + V_{nn}) \Psi_{2n} = E_{2n} \Psi_{2n} \quad (8)$$

The energy obtained for the g.s. corresponds to  $S_{2n}$ . The  $n$ - $n$  potentials are density dependent, zero range forces. The core- $n$  potentials contain central (Woods-Saxon or Gaussian) and spin-orbit terms, and are fitted to reproduce known resonances in the core- $n$  channel.

Two models [29, 30] follow this scheme [Fig. 12(a)], but differ in the way  $\Psi_{2n}$  is expanded. The choice is more intuitive in [29], where the wave functions used are the one-neutron resonant states in the core

potential:

$$\Psi_{2n}^{J\pi} = \sum_{ij} c_{ij} |\phi_{cn}^i \otimes \phi_{cn}^j\rangle_{J\pi} \quad (9)$$

The low-energy continuum neutron states are approximated as discrete states in a radial box of several tens of fm.

A conceptually less evident method is adopted in [30]. The two-neutron problem is solved on a Lagrange mesh, formed by  $N$  points  $x_i$  associated to a set of  $N$  indefinitely derivable functions  $f_i$ . The advantage? The functions are analytical (a polynomial multiplied by an exponential) and they vanish at all mesh points but one [ $f_i(x_j) \propto \delta_{ij}$ ]. The core- $n$  basis is defined by:

$$\phi_{cn} = \sum_i^N c_i f_i(r/h) Y_l(\Omega) \quad (10)$$

where  $h$  is a non-linear parameter aimed at adjusting the mesh to the domain of physical interest. The matrix elements are also analytical [30]. The two-neutron wave function is then constructed as in Eq. (9). In both models, the diagonalization of the hamiltonian [Eq. (8)] provides the energies and admixture coefficients  $c_{ij}$  of the two-neutron states of spin  $J$  and parity  $\pi$  [29, 30]. The g.s. of all Borromean haloes known corresponds to  $0^+$  states.

### Hyperspherical harmonics

Another “family” of three-body models uses Jacobi coordinates [Fig. 12(b)] and expands  $\Psi_{2n}$  on hyperspherical harmonics [4, 31]:

$$\Psi_{2n}^{J\pi} = \rho^{-5/2} \sum \chi_{Kl_x l_y}^{LS}(\rho) |\mathcal{Y}_{KL}^{l_x l_y}(\Omega_5) \otimes X_S\rangle_{J\pi} \quad (11)$$

where  $\rho = \sqrt{x^2 + y^2}$  is the *hyperradius* and  $K = 2n + l_x + l_y$  is the *hypermoment*. Both choices seem to complicate the problem, but both present advantages. Concerning the coordinates,  $\rho$  is a good one-variable measure of the spatial extent of the three-body system.

The expansion provides the explanation of Borromean binding — at least part of it. If we insert Eq. (11) in Eq. (8), the radial Schrödinger equation at large distances  $\rho$  — where the short-range potentials vanish — reads [31]:

$$\left[ -\frac{d^2}{d\rho^2} - \frac{2mE}{\hbar^2} + \frac{(K+3/2)(K+5/2)}{\rho^2} \right] \psi(\rho) = 0 \quad (12)$$

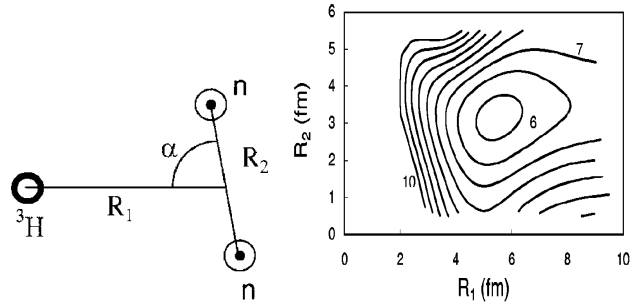


Figure 13: Three-cluster structure assumed for  ${}^5\text{H}$  and energy surface of the  ${}^3\text{H}+n+n$  system in a GCM calculation [33].

Even without binary binding and with total angular momentum  $K = 0$  ( $s$ -waves in the binary subsystems), the three-body centrifugal barrier does not vanish, as the “effective” angular momentum of the system is  $K+3/2$  [4].

Another advantage is that the asymptotic wave function is a generalization of binary scattering to  $3 \rightarrow 3$  scattering [32], modified to take into account the Pauli blocking from the occupied states in the core [4]. Therefore, the asymptotics, which play a leading role in processes involving these nuclei, are properly taken into account. For large values of  $\rho$ , the three-body wave function takes a form similar to Eq. (2):  $\psi(\rho) \propto e^{-\alpha\rho}/\rho$  [4].

There are, however, two similarities with the previous models [Fig. 12(a)] that are not easy to see among these new coordinates and formulae: the core is still inert and the core- $n$  effective potential is still a modified Woods-Saxon or Gaussian [4].

### Generator coordinate method

This model (GCM) gives one step forward, it considers the  $A$  nucleons in the problem [33]:

$$H = \sum_i^A T_i + \sum_{i<j} V_{ij} \quad (13)$$

The main input of the calculation is a  $N$ - $N$  **interaction**,  $V_{ij}$ , instead of the effective  $V_{cn}$  and  $V_{nn}$  potentials used above. This interaction [33, 34] is, however, a simple one compared to the high accuracy fits used in ab initio calculations [12, 35].

The  $A$  nucleons are described by harmonic oscillator (HO) wave functions, which a priori do not seem to be the best choice for very extended and dilute systems. Moreover, the same HO parameter

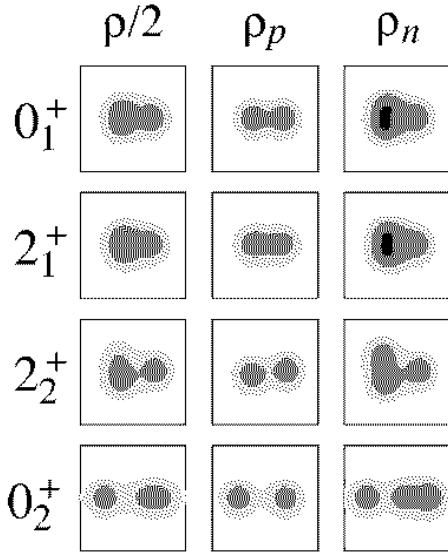


Figure 14: Density distributions of matter, protons and neutrons for intrinsic states in  $^{10}\text{Be}$  obtained from an AMD calculation [36].

is used for all nucleons in order to avoid spurious c.m. problems [34]. The fact that halo nuclei exhibit two distinct phases is taken into account through the introduction of generator coordinates (Fig. 13), which define the centers of the nucleon wave functions. The basis functions of the core- $n$ - $n$  system read:

$$\Phi_{\nu_1\nu_2\nu_3}(R_1, R_2, \alpha) = \mathcal{A}\{\phi_c^{\nu_1}\phi_n^{\nu_2}\phi_n^{\nu_3}\} \quad (14)$$

where  $\mathcal{A}$  is the  $A$ -nucleon antisymmetrization operator. Therefore, even if we deal with an  $A$ -nucleon problem, an a priori clusterization of nucleons within a core has to be assumed.

The total wave function of the system is:

$$\Psi^{J\pi} = \sum_{\substack{R_1 R_2 \alpha \\ \nu_1 \nu_2 \nu_3}} f_{\nu_1\nu_2\nu_3}^{J\pi} \Phi_{\nu_1\nu_2\nu_3}^{J\pi}(R_1, R_2, \alpha) \quad (15)$$

The generator functions  $f^{J\pi}(R_1, R_2, \alpha)$  are then calculated in a grid of generator coordinates [33, 34], and energy surfaces as a function of some coordinates can be constructed (Fig. 13). An advantage of this model is that it takes easily into account excited states of the core [34].

### Antisymmetrized molecular dynamics

This model (AMD) is presented as a probe of how clustering “emerges” (Fig. 14) from the  $A$ -nucleon system without assumptions [36]. The hamiltonian

of the system reads:

$$H = \sum_i^A T_i + \sum_{i<j} V_{ij} + \sum_{i<j<k} V_{ijk} \quad (16)$$

The basis function of the system is a Slater determinant of  $A$  Gaussian wave packets:

$$\Phi_{\text{AMD}}(X_i, \nu) = \mathcal{A}\{\phi_1, \phi_2, \dots, \phi_A\} \quad (17)$$

where  $\nu$  is the width and  $X_i$  the coordinates of the centers. The total wave function of the system is a superposition of AMD wave functions:

$$\Psi^{J\pi} = \sum_j c_j \Phi_{\text{AMD}}^{J\pi}(X_i^j) \quad (18)$$

where the coefficients are obtained by minimizing the energy of the system [36].

With respect to GCM, no clusters are assumed [Eq. (17)]. The notion, however, of halo or valence neutrons becomes less evident since nucleons are no longer labelled — the wave function of the system is a Slater determinant. A standard technique transforms the single particle  $\phi_i$  into an orthonormal base, and leads to single-particle energies. The two highest neutron orbits are then considered as the ones corresponding to the valence neutrons [36].

The hamiltonian [Eq. (16)] seems much more complete than the previous ones. The interaction part is, however, very close to GCM [Eq. (13)]. The  $N$ - $N$  interaction is similar, and the three-body term is just a one-parameter contact interaction:  $V_{ijk} = v_3 \delta(r_i - r_j)\delta(r_i - r_k)$  [36]. Moreover, the appearance of clustering depends much on the choice of  $V_{NN}$  [37]. As it was the case in GCM, the wave functions (Gaussians) are not well adapted to the description of very extended and dilute nuclei.

### Quantum Monte Carlo (ab initio)

These calculations (QMC) use a hamiltonian as complete as AMD [Eq. (16)]:  $A$  nucleons and two- and three-nucleon interactions. The differences are all in favour of QMC [38]:

- the wave functions are more realistic than Gaussians;
- the two-nucleon interactions are parametrizations containing of the order of 60 parameters that fit all known  $NN$  scattering data with a  $\chi^2/\text{datum} \approx 1$  [1];
- the three-nucleon interactions include two-pion exchange processes between three nucleons.

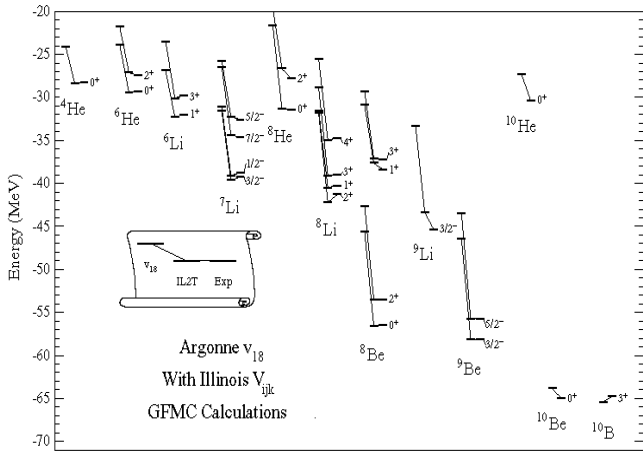


Figure 15: Energy levels of light nuclei from a QMC calculation compared to the experimental ones [12].

These are also known as *ab initio* calculations, since they are believed to be the best ones that can be done today for the description of nuclei in terms of the interactions between nucleons.

The technique used to solve the hamiltonian is Green’s function Monte Carlo (GFMC) [38]. A trial function  $\Psi_T^{J^\pi}$  is first constructed and optimized, and then it is used as the starting point for a GFMC calculation, which projects out the exact lowest energy state with the same quantum numbers by propagation in imaginary time:  $\Psi_0 = \lim_{\tau \rightarrow 0} \exp[-(H - E_0)\tau] \Psi_T$  (for details see [3, S. Rombouts]).

The results, when a “convenient” three-body force is used, are in agreement at the MeV level with energies of light nuclei up to  $A = 10$  (Fig. 15). One should, however, keep in mind that when these calculations are quoted as “*exact at the 1–2% level*” this refers only to the  $V_{ij}$  interaction and to the projection of the lowest energy state corresponding to a given trial function. The construction of the trial function itself before the calculation and the three-body force are not *ab initio* nor *exact* at all.

## 2.4 Beyond two neutrons

We have seen that since their discovery many steps have been undertaken, both experimentally and theoretically, in the understanding of two-neutron haloes. New characteristics have been probed, though roughly, while others remain still out of reach. The coming years will see how techniques like transfer reactions, radiative capture or interferometry analyses will increase their resolving power, and certainly how new techniques will be applied to these systems. But

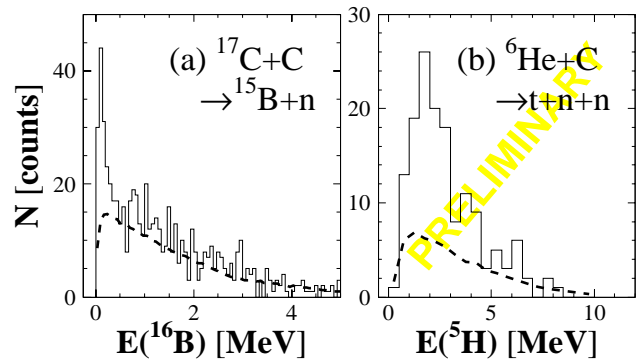


Figure 16: Final state energy for proton-removal reactions on a carbon target: (a)  $^{17}\text{C} + \text{C} \rightarrow ^{15}\text{B} + n$  [40]; (b)  $^6\text{He} + \text{C} \rightarrow t + n + n$  [41]. The dashed lines correspond to the non-resonant background obtained by event mixing (see text).

before going on to the next subject we will discuss three items related to two-neutron halo nuclei.

### Formation of unbound nuclei

In the calculation of core- $n$ - $n$  systems through any of the models described in Sec. 2.3 there is an essential “subproblem”: the core- $n$  system. For some of them it is an input, and for the others is an output that has to be checked. The obvious way to probe it is the study of the resonances in the system by neutron scattering on the core nucleus, but this technique can be only applied to  $^6\text{He}$ , the other Borromean systems having an unstable core.

The most widely used technique is the formation of the system in a binary reaction of the type  $A(\text{B}, \text{core} + n)\text{X}$ . If  $X$  is detected, the missing mass provides the energy of the core+ $n$  system, where peaks can be associated to resonances. The background, however, from reactions on target impurities, for which the partner of  $X$  is not the core+ $n$  system, has to be subtracted [39]. The corresponding  $\ell$  values can be indirectly inferred, if the resolution is high enough, from the width of each peak: for higher  $\ell$  the centrifugal barrier is higher, the life time longer, and the width narrower.

The alternative technique is the coincidence detection of the core and a neutron [Fig. 16(a)]. The energy spectrum is *exactly* the missing-mass one obtained by detecting  $X$ , except for a possible contamination from neutrons stemming from  $X$ , which is not detected. And experimentally is much more complex to detect a fragment and a neutron than just a fragment. What is then the advantage? First,

we *detect* the system, and backgrounds from other reactions are thus absent. Second, we have access to correlations between core and neutron.

The analysis of correlations in the relative angle provides the  $\ell$  of the resonances [42]. Furthermore, the analysis of *energy correlations* extracts the resonances from the background. Not only from the one created by the core and a neutron from  $X$ . The core and the neutron, as well as in experiments detecting  $X$ , can always be produced even if there are no resonances in the system, and the relative energy could exhibit peaks that correspond to pure kinematics, or to correlations in the initial state. These effects lead to a “non-resonant background” [43], which can be obtained from the data by mixing cores and neutrons from different events. Peaks above this contribution *do* correspond to core- $n$  resonant states: for example, the narrow peak in Fig. 16(a) is assigned to a  $d$  resonance, probably the g.s. of  $^{16}\text{B}$ , at  $85 \pm 15$  keV [40].

### Well beyond the drip lines

Core- $n$  systems are just holes before the end point of isotopic chains. Can we go (significantly) beyond the end point? The only such cases that have been studied are superheavy isotopes of hydrogen and helium. The most extreme examples are the observation of resonances that have been attributed to the g.s. of  $^5\text{H}$  (by missing mass [44]) and  $^{10}\text{He}$  (both by missing mass [45] and  $^8\text{He}+n+n$  coincidences [46]).

The same resonance in  $^5\text{H}$  has been recently observed by detecting  $t+n+n$  coincidences [Fig. 16(b)] in proton removal from  $^6\text{He}$  [41]. The analysis of two- and three-body correlations presented in Sec. 2.2 is in progress. Importantly, the parameters extracted such as  $r_{nn}^{\text{rms}}$  or  $\tau$  of resonances in  $^4\text{H}$  (if present) should not be distorted at all by the reaction mechanism, since  $^5\text{H}$  is formed during the reaction and it decays *spontaneously* in the final state.

### May many-neutron haloes exist?

Is the number of halo neutrons limited to 2? We know already that  $^8\text{He}$  is not a three-body system, as  $^6\text{He}$  is too weakly bound to act as a core. The properties of this nucleus are better described by four neutrons around the  $\alpha$  particle [47, 48]. Whether this extremely neutron-rich system is a four-neutron *halo* or not is still subject of debate due to its unexpectedly strong binding — 1.1 MeV more than  $^6\text{He}$  — (Sec. 4).

Two very simple arguments, applied to  $^{11}\text{Li}$ , are presented in [31]. The first one considers the effect

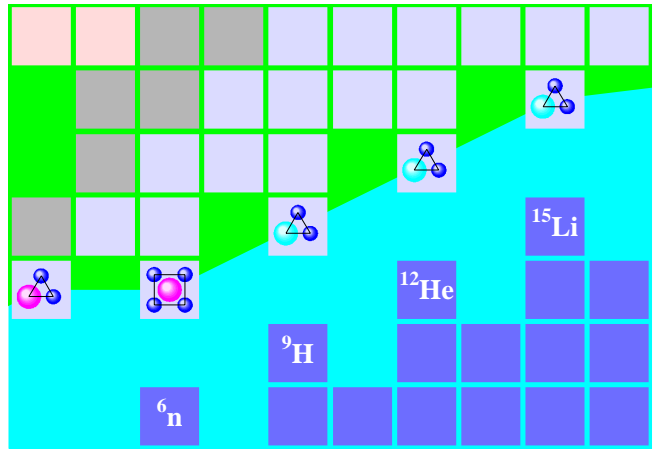


Figure 17: Location in the Segré chart of hypothetical “hyperheavy” particle-stable isotopes beyond the known drip line.

of neutron pairing. The core nucleus is not able to bind each of the neutrons separately, and thus the energy of the system would be, in the absence of neutron pairing, twice the energy of resonances in  $^{10}\text{Li}$ :  $+2\varepsilon_{9n}$ . However, the energy provided by the  $n$ - $n$  interaction,  $-\varepsilon_{nn}$ , is stronger and binds  $^{11}\text{Li}$ . If we extend this argument to  $x$  neutrons added to  $^9\text{Li}$ , the energy of the system would be:

$$E(^{9+x}\text{Li}) = +\varepsilon_{9n} x - \varepsilon_{nn} x(x-1)/2$$

which could be negative for a given  $x > 2$ . Considering that all possible  $n$ - $n$  pairs will interact equally is presumably an overestimate but, even without the  $(x-1)$  factor, the superheavy lithium isotope would be bound if  $2\varepsilon_{9n} < \varepsilon_{nn}$ . This is already true for  $x = 2$ ; higher values, however, would require the presence of enough low-energy resonances in  $^{10}\text{Li}$ .

The same argument can be also extended to dineutron clusters. Excited states in  $^{11}\text{Li}$  are unbound, and could be considered as resonances of energy  $+\varepsilon_{9(2n)}$ . If we add a second dineutron, the energy of the system could become negative:

$$E(^{13}\text{Li}) = +2\varepsilon_{9(2n)} - \varepsilon_{(2n)(2n)}$$

provided that the attraction, now between the two dineutrons, is strong enough. Of course, clusters of more than two neutrons could be also considered. If specific numbers of neutrons correlate better than others (Sec. 4), new superheavy isotopes could form particle stable “reefs” far off the drip line [49] (Fig. 17).

### 3 Nuclear molecules

The term nuclear molecule has long been reserved for dinuclear systems in which two clusters orbit one another. Already in 1960 narrow resonances were observed in  $^{12}\text{C}+^{12}\text{C}$  scattering [50]. The widths were about 100 keV and the energies linear with  $J(J+1)$ , indicating that the system lived long enough to undergo several rotations. The formation of these molecular structures is somehow linked to the stability of the cluster components and to symmetries of the deformed potential describing the composite system, but is not well understood yet [51].

These properties give rise for example to  $\alpha+\alpha$  orbiting in unbound  $^8\text{Be}$ , on the g.s. of which a rotational band is built. Nucleons added to this highly clustered system find themselves in two-center orbits, giving rise to **molecules** fundamentally different from those observed in scattering resonances [52, 53].

Two-center orbits are very similar to those of electrons in covalent bonds in atomic molecules. Moreover, the exchange of these valence nucleons between the two  $\alpha$  clusters can provide additional stability, effectively binding the  $\alpha$  “nuclei” (Fig. 18). The role of nuclei in a molecule played by the  $\alpha$  particles is related to their strong stability and the weakness of the  $\alpha$ - $\alpha$  interaction.

Therefore, there seems to be an analogy between atomic and the latter nuclear molecules. If one considers the characteristics of the problem, however, the differences are huge: relative masses and distances, interaction, substructure of constituents... We will first review the different concepts using atomic (“true”) molecules, and see how the link can be made through the molecular orbitals of the systems. These will be obtained with a very simple model: the deformed harmonic oscillator. Finally, the increasing complexity of the molecules studied will be addressed.

#### 3.1 True molecules

We will review here chapters 6,7 of [54], in which the hydrogen atom is used as the starting point for the description of more complex atoms and diatomic molecules.

##### Atoms

The most simple example of an atomic system is the one-electron atom (hydrogen or hydrogen-like ions).

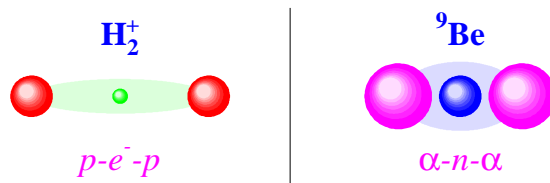


Figure 18: Sketch of the analogy between the  $\text{H}_2^+$  molecule, bound by the electron, and the  $^9\text{Be}$  nucleus, bound by the neutron added to  $^8\text{Be}$ .

The hamiltonian and energies of this two-body system bound by the Coulomb interaction are, in atomic units:

$$H = -\frac{1}{2}\nabla^2 - \frac{Z}{r} \quad (19)$$

$$E_n = -\frac{Z^2}{2n^2} \quad (20)$$

The wave functions  $\phi_H(n, \ell, m)$  lead to the hydrogen orbitals  $s, p, d, \dots$  for  $\ell = 0, 1, 2, \dots$  (Fig. 20, middle row). From the nuclear perspective one could expect that atomic physics is an “exact science”, since it deals with point-like particles bound by a simple interaction. The hydrogen atom is, however, the *only* problem with an exact solution!

The next problem is the helium atom (Fig. 19). The hamiltonian is:

$$H = -\frac{1}{2}[\nabla_1^2 + \nabla_2^2] - \frac{2}{r_1} - \frac{2}{r_2} + \frac{1}{r_{12}} \quad (21)$$

It has no exact solution anymore due to the electron repulsion (three-body problem). One way out is to neglect this term and take it effectively into account by introducing an effective charge (we are getting closer to nuclear physics...):

$$H' = -\frac{1}{2}[\nabla_1^2 + \nabla_2^2] - \frac{Z'}{r_1} - \frac{Z'}{r_2} \quad (22)$$

which is the nuclear charge minus the screening of the other electron. Eq. (22) is the sum of two one-electron problems, and therefore the solution can be written as:

$$\Psi = \phi_H(1) \phi_H(2) \quad (23)$$

$$E = -\frac{Z'^2}{2} \left( \frac{1}{n_1^2} + \frac{1}{n_2^2} \right) \quad (24)$$

Using the exact hamiltonian and minimizing the energy leads to  $Z' = Z - \frac{5}{16}$ , which gives a binding energy only 2% higher than the experimental value.

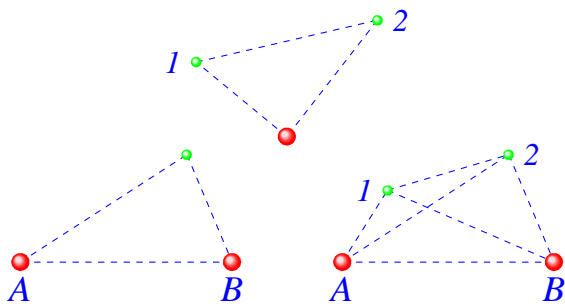


Figure 19: The simplest problems beyond one-electron atoms: the helium atom (top) and the  $\text{H}_2^+$  and  $\text{H}_2$  molecules (bottom).

In this way one can construct an independent electron theory for atoms with  $N$  electrons by neglecting the  $N(N-1)/2$  repulsion terms:

$$H' = -\frac{1}{2} \sum_i^N \nabla_i^2 - \sum_i^N \frac{Z'}{r_i} \quad (25)$$

$$\Psi = \prod_i^N \phi_H(i) \quad (26)$$

where  $Z'$  is now the nuclear charge screened by the  $N-1$  other electrons.

## Molecules

The simplest molecule is  $\text{H}_2^+$  (Fig. 18). In the same way that the solutions of the hydrogen atom are used in constructing an approximate theory of more complex atoms, the solutions of this problem can be used to develop an approximate theory of more complex diatomic molecules.

The hamiltonian (Fig. 19) is:

$$H = -\frac{1}{2} \sum_i \nabla_i^2 - \frac{1}{r_A} - \frac{1}{r_B} + \frac{1}{R_{AB}} \quad (27)$$

Again we have a three-body problem, but now we cannot replace the proton repulsion by an effective screen. There is, however, another approximation (called Born-Oppenheimer) that can be made: the motion of electrons in a molecule is so rapid that the nuclei may be regarded as fixed. We can thus solve the problem for a set of internuclear distances and then plot the energy of the molecule as a function of  $R_{AB}$ : the minimum in the curve corresponds to the configuration of the stable molecule.

The Born-Oppenheimer approximation eliminates also the nuclear kinetic terms, and Eq. (27) becomes a one-electron problem. It is exactly soluble, but

there is an approximate solution that illustrates well the variational principle and the method of linear combination of atomic orbitals (LCAO). The variational principle states that “the expectation value of the energy calculated from any approximate wave function will always be higher than the true energy of the g.s.”. Therefore, we can propose several trial wave functions and choose the one with the lowest energy as the best approximation among the ones proposed.

A more systematic procedure is to use one trial function but with several arbitrary parameters, with respect to which the energy is minimized. Therefore, a huge number of guesses is made with only one function, but the solution will be *just* the best one within the particular parametric form chosen. The trial function is usually a linear function, and this is the basis of the LCAO method. Since molecules are made up of atoms, it is reasonable to assume that the electron distribution in a molecule can be approximated by a sum of atomic electron distributions.

For example, we can approximate the molecular orbitals  $\Psi$  of  $\text{H}_2^+$  by a linear combination of hydrogen  $1s$  orbitals  $\phi$ . The minimization of the energy leads to:

$$\Psi_{\pm} = (\phi_A \pm \phi_B) \quad (28)$$

Applying Eq. (27) to this wave function leads to:

$$E_{\pm} = \langle \phi_A | H_A | \phi_A \rangle + \langle \phi_B | H_B | \phi_B \rangle + \left\{ \frac{1}{R_{AB}} - 2 \langle \phi_A | \frac{1}{r_B} | \phi_A \rangle \right\} \mp \langle \phi_A | H | \phi_B \rangle \quad (29)$$

The first line corresponds to the energy of each atom. Next there is the Coulomb term, in which the extra attraction of each electron by the other proton at short internuclear distances is overwhelmed by the proton repulsion. Finally, there is the **exchange term**, that takes into account the fact that electrons are not restricted to atom  $A$  or  $B$  but can exchange places between the two orbitals. This term provides the stability of the molecule for the  $\Psi_+$  orbital.

We can now add another electron and calculate the solutions of the  $\text{H}_2$  molecule (Fig. 19). Four terms must be added to Eq. (27): kinetic term, attraction by the two protons, and repulsion by the other electron. By adding  $\pm 1/R_{AB}$ , the hamiltonian can be rewritten:

$$H = H^+(1) + H^+(2) - \frac{1}{R_{AB}} - \frac{1}{r_{12}} \quad (30)$$

where  $H^+$  is the hamiltonian for the electron in  $\text{H}_2^+$ . If we neglect the electron repulsion and fix the internuclear distance, Eq. (30) is twice a one-electron

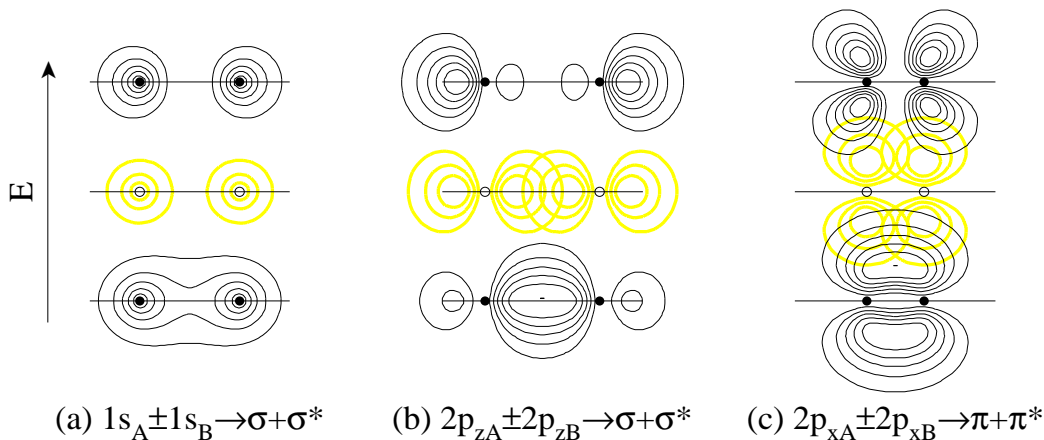


Figure 20: The formation of molecular orbitals  $\Psi_{\sigma,\pi}$  from linear combinations of atomic hydrogen orbitals  $\phi_{s,p}$  of atoms  $A$  and  $B$ . From top to bottom:  $|\Psi_i^*|^2$  (antibonding orbital),  $|\phi_i|^2$  (the two atomic orbitals) and  $|\Psi_i|^2$  (bonding orbital), all projected in the  $XZ$  plane. Symbols correspond to the location of the atomic nuclei.

problem. The wave function can thus be written as  $\Psi = \Psi_+(1)\Psi_+(2)$ , where  $\Psi_+$  is the wave function of each electron in  $\text{H}_2^+$  [Eq. (28)]. We can expand the wave function following several approximations (first/second function refers to electron 1/2):

$$\Psi = \phi_A\phi_B + \phi_B\phi_A + \phi_A\phi_A + \phi_B\phi_B \quad (31)$$

$$\approx \phi_A\phi_B + \phi_B\phi_A \quad (32)$$

$$\approx \phi_A\phi_B + \phi_B\phi_A + \lambda(\phi_A\phi_A + \phi_B\phi_B) \quad (33)$$

$$\approx \Phi_A\Phi_B + \Phi_B\Phi_A \quad [\Phi = 1s + \lambda 2p] \quad (34)$$

In Eq. (31) the third and fourth terms represent the probability of finding both electrons close to one nucleus, and are called ionic terms ( $\text{H}_A^+\text{H}_B^-$  and  $\text{H}_A^-\text{H}_B^+$ ). The corresponding energy of the molecule is off by 6.4%. This wave function is contrary to experience because the ionic terms predict that one half of the hydrogen molecules should dissociate into the ions  $\text{H}^+$  and  $\text{H}^-$ , and this is never the case.

Therefore, the second approximation is to keep only the covalent terms [Eq. (32)]. The error in the energy decreases to 4.9%. It seems thus better to omit the ionic terms than to take them with equal weight. It might then be that introducing them multiplied by a variational parameter leads to a better wave function [Eq. (33)]. Minimizing the energy leads to  $\lambda = 0.25$  and the energy is now off by 4.7%.

Does this mean that the wave function is an ionic-covalent mixing? No. We can use another approach [Eq. (34)] without ionic terms but with a basis hydrogen orbital with a little  $2p$  character (an *hybrid* orbital). Minimizing the energy with respect to  $\lambda$  gives a binding energy only 4.2% higher than the experi-

mental value. This is the best result of the four. Does this mean that hydrogen atoms are slightly “polarized” in  $\text{H}_2$  and that the molecule is purely covalent? No!

It means just that adding terms with variational parameters leads always to a better description of the observables. The best wave function of  $\text{H}_2$  is a 50 term variational function, in which all the concepts of atomic and molecular orbitals, Coulomb and exchange terms, or polarization of the atoms disappear [54]: “*it is still an open question whether accurate, ab initio calculations will solve fundamental problems associated with the structure of complex molecules*”. This question can be extended to nuclear physics.

## Molecular orbitals

Molecular orbitals that can be constructed by simple linear combinations of atomic hydrogen orbitals are displayed in Fig. 20. They are named depending on the component of angular momentum about the bond axis ( $Z$  in the figure):  $\sigma, \pi, \delta, \dots$  for  $m = 0, \pm 1, \pm 2, \dots$ , respectively. The LCAO method always leads to as many molecular orbitals as the number of basis orbitals. At the equilibrium internuclear distance, one of the molecular orbitals has an energy lower than the isolated atoms (bonding) and the other has a higher energy (antibonding, marked with an asterisk).

Bonding (antibonding) orbitals keep the electrons in (out of) the region between the two nuclei (Fig. 20). An identical pair of  $\pi, \pi^*$  orbitals can be constructed with  $2p_{yA} \pm 2p_{yB}$ . The stability of the



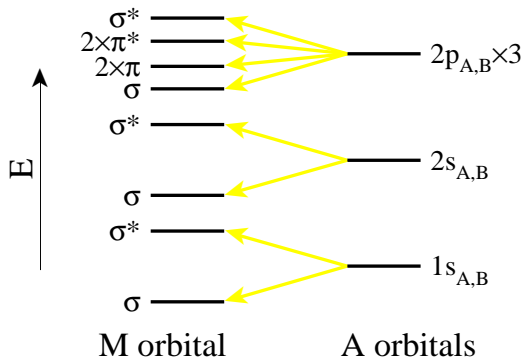


Figure 21: Energies of diatomic molecular orbitals constructed in MO theory from the atomic orbitals in atoms  $A$  and  $B$  [54].

molecule can be predicted by the number of bonding and antibonding orbitals filled. The order of the orbital energies for molecules with large internuclear distances is shown in Fig. 21. For a molecule being stable there has to be an overall extra binding with respect to the two isolated atoms. Therefore, molecules like  $\text{He}_2$  or  $\text{Be}_2$  do not exist [54, p. 166].

### 3.2 The nuclear concepts

In the sketch of Fig. 18 the atomic and nuclear problems seem analog. The simple arguments we have followed in the atomic case, however, do not seem evident at all to translate into the nuclear case. There are no basis, exact functions like the hydrogen ones, the “nucleus-electron” interaction is poorly known, the finite size and motion of “nuclei” in the molecule cannot be neglected... How are the different concepts translated?

#### Born-Oppenheimer approximation

In atomic molecules, the internuclear distance was fixed and the problem was solved for a series of values, mapping the evolution of the molecule energy with  $R_{AB}$ . In nuclear molecules of the type  $A^{>8}\text{Be}$  we cannot freeze the two  $\alpha$  particles, but we can mimic the Born-Oppenheimer approximation by using a two-center potential (created by the  $\alpha$  particles) for the valence neutrons, and solve de Schrödinger equation for several interpotential distances.

This is done in the two-center shell model (TCSM) [55, p. 571] and the two-center harmonic oscillator (TCHO) [56]. The TCHO case is shown in Fig. 22. For effectively infinite separation the associated energy levels are degenerate, the quantum numbers are

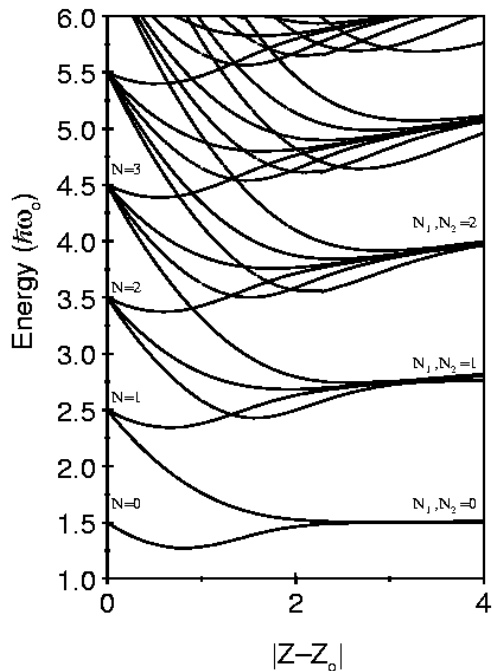


Figure 22: The energy levels of the two-center harmonic oscillator as a function of the separation of the two potentials from the origin  $Z_0$  (the interpotential distance is  $2|Z - Z_0|$ ) [51].

equal. As the two wells overlap the degeneracy is removed with some levels being pushed up, and others down, due to the Pauli principle: two identical initial wave functions (with respect to different centers) must evolve into two different wave functions (with respect to a common center).

For example, two  $N = 0$  (nodeless) wave functions fuse to form an  $N = 0$  state and, in addition, create a node along the interpotential axis ( $N = 1$ ). This resembles much the evolution shown in Fig. 21 from isolated atomic orbitals to common molecular orbitals.

#### The LCAO method

The use of linear combination of atomic orbitals has its analog in the LCNO (linear combination of nuclear orbitals) approach [57], which describes the effect that can be expected from the exchange of a nucleon, as was discussed in Eq. (29) for an electron.

A clear example is given in [58].  $^{20}\text{Ne}$ , as will be seen below, has a pronounced  $^{16}\text{O}-^4\text{He}$  cluster structure. The two clusters are particularly stable and their relative interaction is weak: the valence neutron in  $^{21}\text{Ne}$  can be considered as a nucleon in the field of the two clusters. Therefore, its wave func-

tion is naturally constructed as a linear combination of “atomic” states of the neutron in  $^{17}\text{O}$  and  $^5\text{He}$ .

### Orbitals

The orbitals corresponding to the valence neutrons in highly clustered systems can be obtained from some of the complex models noted above, like TCSM, TCHO or AMD. Their shape is in fact very similar to the one of the analytical LCAO orbitals shown in Fig. 20. We will see that the deformed harmonic oscillator leads to analytical nuclear orbitals and that these resemble also to the  $\sigma$  and  $\pi$  atomic ones.

Another concept which is translated into nuclear physics, not necessarily in the molecular context, is that of hybrid orbitals [54, p. 180]. In molecules formed with  $p$  atomic orbitals the angles between bonds should correspond to the angle between the three  $p_{x,y,z}$  orbitals,  $90^\circ$ . Experimentally, the angles are higher:  $104.5^\circ$  in  $\text{H}_2\text{O}$ ,  $108^\circ$  in  $\text{NH}_3$ ,  $120^\circ$  in  $\text{BCl}_3$ , or even  $180^\circ$  in  $\text{HgCl}_2$ .

Instead of using pure  $p$  orbitals, atoms *hybridize* one  $s$  and  $x$   $p$  orbitals to form  $x + 1$   $sp^x$  orbitals. For  $sp^{3,2,1}$  the bond angles are  $109$ ,  $120$  and  $180^\circ$ , respectively, which correspond to the  $\text{NH}_3$ ,  $\text{BCl}_3$  and  $\text{HgCl}_2$  examples noted above. In nuclei, the wave function of nucleons is represented also as an hybridization of different single-particle wave functions, weighted by spectroscopic factors.

### 3.3 Deformed harmonic oscillator

Two-center models provide an appropriate description of fission of cluster states into their constituents and also of fusion of nuclei into a compound system (Fig. 22 from left to right and vice versa). The existence of clusters is, however, assumed through the definition of the two potentials.

The deformed harmonic oscillator model, even if inadequate for a detailed description of nuclear properties due to its infinite parabolic behaviour, is useful in many senses:

- calculations of wave functions and densities are analytical and simple;
- shell structure, even without spin-orbit coupling, is fairly well reproduced for light nuclei;
- it is a single potential, without clustering assumptions.

The spherical HO potential,  $V = \frac{1}{2}m\omega_0 r^2$ , leads to energy shells  $E = \hbar\omega_0(N + 3/2)$ . The axially

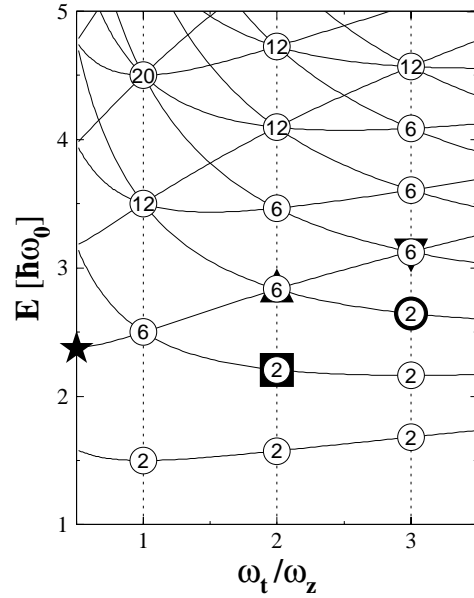


Figure 23: The deformed HO energy levels. The numbers inside the circles indicate the degeneracies at level crossings, and the closed symbols the higher occupied level that could be associated to some deformed,  $N = Z$  “closed shell” nuclei:  $^{12}\text{C}_{\text{gs}}$  (★),  $^8\text{Be}$  (■),  $^{20}\text{Ne}$  (▲),  $^{12}\text{C}_{0^+}$  (●) and  $^{24}\text{Mg}$  (▼).

symmetric HO potential (only prolate and oblate deformations) removes this degeneracy [5, p. 418]:

$$V = \frac{1}{2} m [\omega_t(x^2 + y^2) + \omega_z z^2] \quad (35)$$

$$E = \hbar\omega_t(n_t + 1) + \hbar\omega_z(n_z + 1/2) \quad (36)$$

Volume conservation ( $\omega_t^2 \omega_z = \omega_0^3$ ), however, leads to **new shells** for integer  $\omega_t/\omega_z$  (or  $\omega_z/\omega_t$ ) values, as shown in the level scheme in Fig. 23.

The three-dimensional density of a nucleus can be calculated from:

$$\rho(\vec{r}) = \sum_{i=1}^A \left| \phi_{n_x}^i \left( \frac{x}{b_x} \right) \phi_{n_y}^i \left( \frac{y}{b_y} \right) \phi_{n_z}^i \left( \frac{z}{b_z} \right) \right|^2 \quad (37)$$

where the one-dimensional HO functions are:

$$\phi_n \left( \frac{x}{b} \right) = \frac{e^{-x^2/2b^2} H_n \left( \frac{x}{b} \right)}{\sqrt{2^n n!} b \sqrt{\pi}} \quad (38)$$

the length parameters are related to the frequencies by  $b^2 = \hbar/m\omega$  and  $H_n$  are Hermite polynomials.

#### The $\alpha + \alpha$ system

Let us consider  $^8\text{Be}$  (Fig. 23). The four protons and neutrons would fill  $N = 0$  and only one third

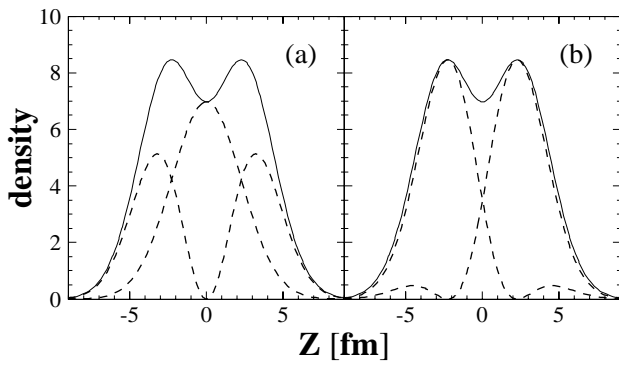


Figure 24: Density of the  ${}^8\text{Be}$  g.s. along the  $Z$  axis for a  $\omega_t/\omega_z = 2$  HO. The dashed lines correspond to: (a) the densities of the HO  $\psi_{00}$  and  $\psi_{01}$  wave functions; and (b) the ones of the two-center  $\psi_A$  and  $\psi_B$  wave functions.

of  $N = 1$ . But, if the system deforms along  $Z$  to  $\omega_z = \omega_t/2$ , the four nucleons would fill two complete levels:  $(n_t, n_z) = (0, 0)$  and  $(0, 1)$ . It would be, therefore, energetically more favourable for the eight nucleon system to be deformed rather than spherical.

The density of  ${}^8\text{Be}$ , calculated in a  $\omega_t/\omega_z = 2$  HO, is plotted in Fig. 24, and exhibits two peaks along the  $Z$  axis. These result from the  $s$  ( $\psi_{00}$ ) and  $p$  ( $\psi_{01}$ ) wave functions, plotted in Fig. 24(a). In Eq. (28) we saw that the molecular functions  $\Psi_{\pm}$  could be constructed from the atomic ones  $\phi_{A,B}$ . We can of course go the other way round<sup>†</sup>:  $\phi_{A,B} = \Psi_{\pm} \pm \Psi_{\mp}$ , and extract the atomic functions from the molecular ones.

This transformation leads here to  $\psi_{A,B} = \psi_{00} \pm \psi_{01}$  [Fig. 24(b)]. Now it seems that  ${}^8\text{Be}$  is made of two spatially separated  $s$  wave functions. Indeed, the overlaps with a pure  $\alpha$ -particle wave function are  $\langle \psi_{A,B} | \phi_{\alpha} \rangle \approx 0.9$ . This interpretation is reinforced by having a look to the density in the  $XZ$  plane (Fig. 25), where the two  $\alpha$  particles are clearly apparent. The deformed HO behaves as two slightly overlapping smaller spherical potentials.

### Molecular (but nuclear) orbitals

Now we can plot the densities of neutrons added on top of  ${}^8\text{Be}$ . The next “shell”, at  $\frac{9}{2}\hbar\omega_z$ , corresponds to the  $(n_t, n_z) = (1, 0)$  and  $(0, 2)$  levels. The shape is *exactly* the one of the covalent bonds  $\pi$  and  $\sigma$  (Fig. 20) obtained by LCAO!

The study of the two valence neutrons in  ${}^{10}\text{Be}$  with

<sup>†</sup>The normalization constants of the wave functions are being omitted for clarity, at least most of the times...

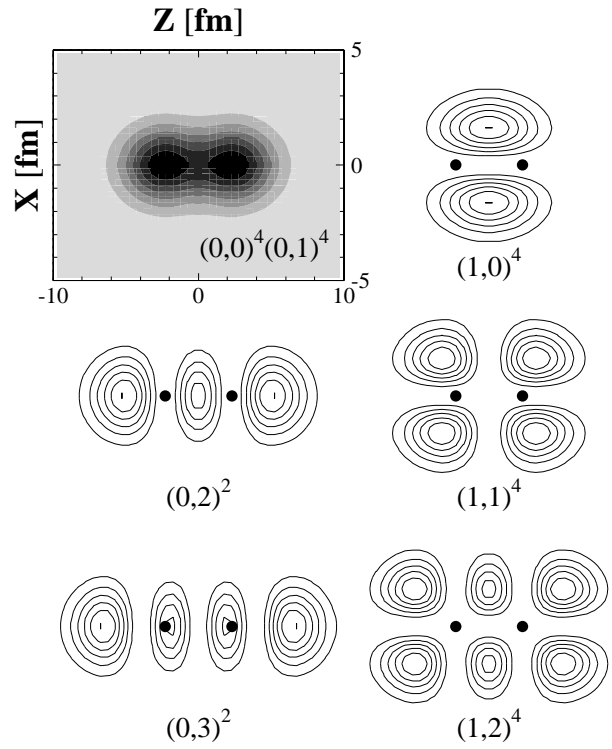


Figure 25: Density of  ${}^8\text{Be}$  for a  $\omega_t/\omega_z = 2$  HO projected onto the  $XZ$  plane. The contour lines correspond to  $(n_t, n_z)$  orbitals in higher shells (Fig. 23): six neutrons in  $(1,0)(0,2)$  at  $\frac{9}{2}\hbar\omega_z$ , six in  $(1,1)(0,3)$  at  $\frac{11}{2}\hbar\omega_z$ , and four of the twelve in the  $(1,2)(0,4)(2,0)$  shell at  $\frac{13}{2}\hbar\omega_z$  — the symbols indicate the two “centers”.

AMD reveals the same shapes, and the results are also interpreted in terms of molecular orbitals [36]. The  $0_1^+$  (g.s.),  $1^-$  and  $0_2^+$  states are associated to configurations  $\alpha+\alpha$  with two neutrons in  $\pi^2$ ,  $\sigma\pi$  and  $\sigma^2$  orbits, respectively. The g.s. is quite compact (Fig. 14) due to the shape of the  $\pi$  orbit: a ring around the axis between the two  $\alpha$  particles.

The link between the binding of these isotopes and the exchange probability of the valence neutrons can be understood as follows: if the  $\alpha$ - $\alpha$  distance increases, the neutrons become more and more localized at one of the centers and raise the kinetic energy (decrease the stability) of the molecule; but, if the  $\alpha$  particles get too close to each other, the neutrons feel the repulsive effect due to the Pauli principle and also raise the kinetic energy of the molecule. The balance between these two effects provides the equilibrium configuration of the molecular state [36, 59].

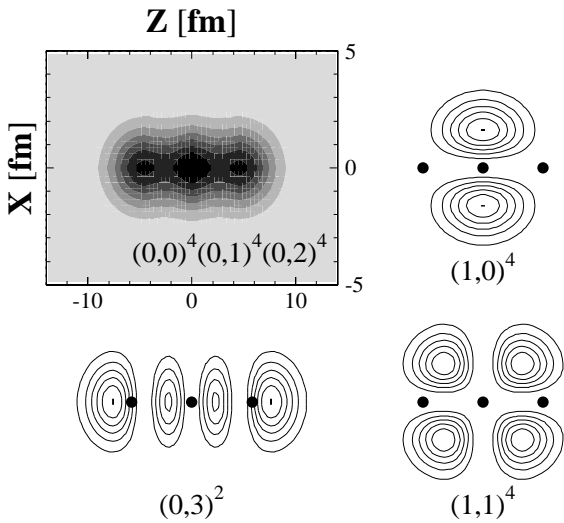


Figure 26: Density of  $^{12}\text{C}$  for a  $\omega_t/\omega_z = 3$  HO projected onto the XZ plane. The contour lines correspond to  $(n_t, n_z)$  orbitals in higher shells (Fig. 23): six neutrons in  $(1,0)(0,3)$  at  $\frac{13}{2}\hbar\omega_z$ , and four of the six in the  $(1,1)(0,4)$  shell at  $\frac{15}{2}\hbar\omega_z$  — the symbols indicate the three “centers”.

### “Many-neutron haloes”?

There might be a curious link between the discussions we had about the possible existence of hyperheavy isotopes (Fig. 17) and the stability conditions for molecules derived from the LCAO method (Fig. 21). The  $(1,0)$  and  $(0,2)$  levels correspond to bonding orbitals and are filled with six neutrons: from  $^9\text{Be}$  to  $^{14}\text{Be}$ , the last beryllium isotope known.

The next six neutrons ( $^{15-20}\text{Be}$ ) go into levels  $(1,1)$  and  $(0,3)$ , the shape of which corresponds to antibonding molecular orbitals — neutrons are pushed away from the region between the  $\alpha$  particles. According to LCAO, these isotopes should not be bound.

However, if the next levels correspond again to bonding orbitals, LCAO would predict neutrons in these orbitals to bind the system, as it happens in molecules:  $\text{Li}_2$  is bound,  $\text{Be}_2$  is not, but  $\text{B}_2$ ,  $\text{C}_2$ ... are bound again (Fig. 21). Indeed, the  $(1,2)$  orbital in Fig. 25 — as well as  $(0,4)$  and  $(2,0)$  — has again a bonding profile. These orbitals would correspond to  $^{21-32}\text{Be}$ !

### Deformation and clustering

We can extend the discussion to nuclear trimers. Historically, the excited  $0_2^+$  state of  $^{12}\text{C}$  at 7.65 MeV — the starting point of stellar nucleosynthesis — has been linked to a  $3\alpha$  chain structure. The chain is

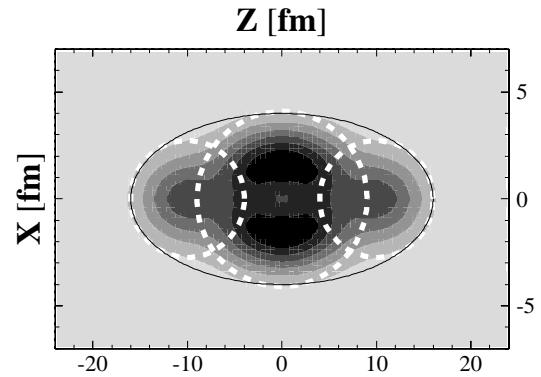


Figure 27: Density of  $^{24}\text{Mg}$  for a  $\omega_t/\omega_z = 3$  HO projected onto the XZ plane. The lines represent the deformed potential (solid) and three spherical overlapping potentials (dashed), which can be related to an  $\alpha$ - $^{16}\text{O}$ - $\alpha$  configuration.

most probably bent [60], though it could be that the bending mode of the pure  $\alpha$  chain gets stabilized once valence neutrons are added [53].

The density of  $^{12}\text{C}$  in a  $\omega_t/\omega_z = 3$  HO potential is shown in Fig. 26, where a linear  $3\alpha$  chain emerges. Neutrons on top of  $^{12}\text{C}$  are placed in  $\sigma$  and  $\pi$  orbitals. Curiously, orbitals beyond those in the figure have an antibonding profile, and thus LCAO predicts that only ten neutrons can be added to  $^{12}\text{C}$ : this takes us to  $^{22}\text{C}$ , the heaviest carbon isotope known...

In view of Figs. 25,26 we can wonder whether clustering emerging from the deformed HO is restricted to  $\alpha$  particles. One could say yes, as in light nuclei the Coulomb interaction is small and each filled pair of proton and neutron levels with common quantum numbers can be associated to an  $\alpha$  particle:  $|2p2n\rangle_{L=0} \equiv |\alpha\rangle$  [51]. Therefore, the clustering observed in Figs. 25,26 should not be considered as a surprise.

But the answer is no! The deformed potential leads to much heavier cluster components. As an example, the description of  $^{24}\text{Mg}$  in a  $\omega_t/\omega_z = 3$  HO leads, as was the case in  $^{12}\text{C}$ , to three spherical cluster components (Fig. 27), but one of them is  $^{16}\text{O}$ . This clusterization could be already expected from the level scheme in Fig. 23: for a  $\omega_t/\omega_z = n$  potential the spherical degeneracies are repeated  $n$  times. The deformed HO behaves as a **series of overlapping potentials** (dashed lines in Fig. 27), each possessing the spherical HO shell structure

The  $N = Z$  nuclei marked in Fig. 23 display well this phenomenon. They are all particularly stable, but none of them would correspond to a closed

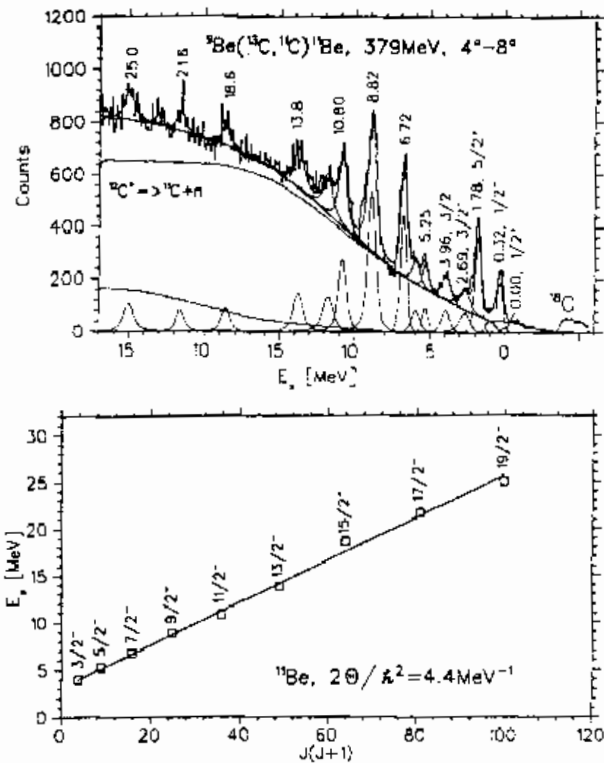


Figure 28: The spectrum of  $^{11}\text{Be}$  states observed in the  $^9\text{Be}(^{13}\text{C}, ^{11}\text{C})^{11}\text{Be}$  reaction (top) and the proposed energy-spin systematics (bottom) consistent with a rotational band [61].

shell configuration in the spherical HO. They find, through deformation, the possibility of closing shells. The oblate  $^{12}\text{C}$  structure corresponds to an equilateral triangular arrangement of three  $\alpha$  particles in the XY plane, while the prolate structure is related to the  $3\alpha$  chain [59]. The prolate  $^{20}\text{Ne}$  structure can be related to an  $^{16}\text{O}-\alpha$  configuration. The  $^8\text{Be}$  and  $^{24}\text{Mg}$  cases have been already discussed.

### 3.4 More complex molecules

Experimentally, these molecular states are probed through the spectrum originated by their rotation. One can thus search, within the known excited states of potential candidate nuclei, for rotational bands that can be interpreted in terms of the rotation of a molecular state [52, 53]. The states involved are at relatively high excitation energy, beyond the cluster emission thresholds, and therefore unbound. The experiments aiming to study these states are then of the same kind than those described in Sec. 2.4: missing mass and coincidence detection of clusters.

An example of missing mass is shown in Fig. 28 for

the reaction  $^9\text{Be}(^{13}\text{C}, ^{11}\text{C})^{11}\text{Be}$ , where the energy of  $^{11}\text{C}$  displays the excited states in  $^{11}\text{Be}$  [61]. Besides the strong background associated to this technique (Sec. 2.4), only the energy is measured, the spin and parity have to be assigned. By assuming that all of the states observed correspond to the population of a band built on the  $3/2^-$  configuration, the energy is linear with  $J(J+1)$ .

The coincidence technique has a negligible background and provides also the spin of the states [62], but it can only “see” states that decay — and maybe only partly — into the clusters considered. Both techniques keep providing complementary information on molecular states.

### Three-center molecules

Fig. 26 shows how the deformed HO predicts the formations of nuclear trimers. The  $^{12}\text{C}_{0_2^+}$  state is just unbound with respect to the  $3\alpha$  threshold, but the role played by successive bonding neutrons may lead to strong  $3\alpha+xn$  molecular configurations in — or close to — the g.s. of very neutron-rich carbon isotopes [53]. No theoretical models, however, describe how the valence neutrons could form these chains.

Experimentally, besides the limited evidence found in the spectrum of  $^{13}\text{C}$  [53], there has been an attempt to explore the  $\alpha \frac{n}{n} \alpha \frac{n}{n} \alpha$  chain structure in  $^{16}\text{C}$  [63]. The breakup of  $^{16}\text{C}$  on a carbon target into  $^8\text{He}+2\alpha$  or  $^6\text{He}+\alpha$  was not observed, and therefore only upper limits to the decay of trimers via the dimer states in  $^{10,12}\text{Be}$  could be estimated.

### More “electrons” in the cloud

Instead of exploring trimers, we can form more complex molecular structures by adding more neutrons to a dimer, easier to handle both theoretically and experimentally. The study of molecular states that are now well established in  $^9-^{11}\text{Be}$  has been recently extended to  $^{12}\text{Be}$  ( $\alpha \frac{nn}{nn} \alpha$ ) and even  $^{14}\text{Be}$  ( $\alpha \frac{nnn}{nnn} \alpha$ ).

The  $\alpha \frac{nn}{nn} \alpha$  states were formed by inelastic excitation of  $^{12}\text{Be}$  on  $^{12}\text{C}$  and  $\text{CH}_2$  targets, and detected through their decay into  $^6\text{He}+^6\text{He}$  and  $^4\text{He}+^8\text{He}$  [62]. The results indicate that breakup of  $^{12}\text{Be}$  occurs from excited states in the 12–25 MeV interval [Fig. 29(top)]. Angular correlations between the clusters provide a model independent spin determination, in the range  $4-8\hbar$ , that indicate the decay of rotational states related to an exotic molecular structure [Fig. 29(bottom)].

The possible  $\alpha \frac{nnn}{nnn} \alpha$  configurations were investigated by breaking up a  $^{14}\text{Be}$  beam into  $^8\text{He}+^6\text{He}$  [64].

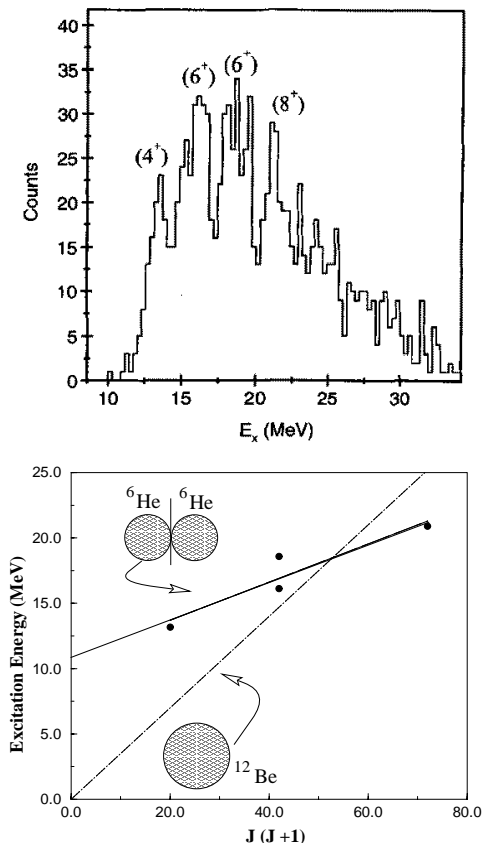


Figure 29: Excitation energy spectrum for states in  $^{12}\text{Be}$  that break up into  ${}^6\text{He}+{}^6\text{He}$  (top) and the energy-spin systematics (bottom) compared to the spherical and two-cluster configurations [62].

Three small peaks were observed in the region 10-16 MeV, but a determination of the spin was not possible.

Similar systematics have been extracted for the isobaric analog states of the beryllium isotopes in  ${}^9\text{-}^{11}\text{B}$  [52, 53]. These are molecules with two kinds of “electrons”, for example  $\alpha \frac{n}{p} \alpha$  in  ${}^{10}\text{B}$ , and it would be interesting to undertake a comparative study of these systems in order to test how the Coulomb interaction modifies the molecular structures found in beryllium.

## 4 Multineutrons

In the two preceding sections we have seen first how several neutrons can virtually “escape” from the nucleus to form a halo and, in the case of  ${}^{6,8}\text{He}$ , how they can associate to other “fugitives” to bind nuclear molecules, the most exotic case being the recently observed  $\alpha \frac{nn}{nn} \alpha$  configurations in  ${}^{12}\text{Be}$ . In both cases we deal with many-neutron systems that exist within a given frame, the nucleus.

A question naturally arises: how would these neutron systems behave in the absence of witnesses (the core in halo nuclei or the  $\alpha$  particles in nuclear molecules)? The debate about the possible existence of neutral nuclei has a long and checkered history that may be traced back to the early 1960s [65]. But forty years later there is only one clear evidence: the dineutron is unbound.

These decades have led to a very long list of experiments and calculations. And there is an overall consensus [66]: experimentally, no one has been able to create and detect multineutrons; theoretically, they should not exist according to our present knowledge of the nuclear interaction. Are these conclusions strong enough to close the multineutron file?

We will try to provide an answer by weighting the different theoretical arguments and the experiments that have been undertaken. We will see how some of the experiments presented in the preceding sections can be extended here to push further the present limits of multineutron (non-)existence, and discuss the first results that suggest the possible existence of  ${}^4n$ .

### 4.1 For and (mostly) against

The different arguments are based on things we know more or less well: the binding energies and structure of  $N \approx Z$  nuclei are extrapolated to  $Z = 0$ , and the  $n$ - $p$  and  $p$ - $p$  interactions are extrapolated to the  $n$ - $n$  system. How valid are these extrapolations?

#### The neutral liquid drop

The most straightforward calculation is setting  $Z = 0$  in Eq. (1): the Coulomb term disappears and the asymmetry term becomes linear with  $A$ . If we neglect the pairing term:

$$B/A \approx (a_v - a_a) - \frac{a_s}{A^{1/3}} \quad (39)$$

The asymptotic binding depends only on the relative value of the volume and asymmetry parameters. The typical values are  $a_v \sim 15$  and  $a_a \sim 23$  MeV [2], and then neutron systems should be unbound by more than 8 MeV/ $N$ .

The asymmetry term in Eq. (1) is obtained from the Fermi gas model by expanding the energy of the  $A$  nucleons around  $N \approx Z$  [2, p. 241]. The results of the standard liquid drop formula are compared to the known nuclear energies in Fig. 30 (solid lines). Even if the lightest  $N = Z$  nuclei are not well described — the set of parameters used here is the standard

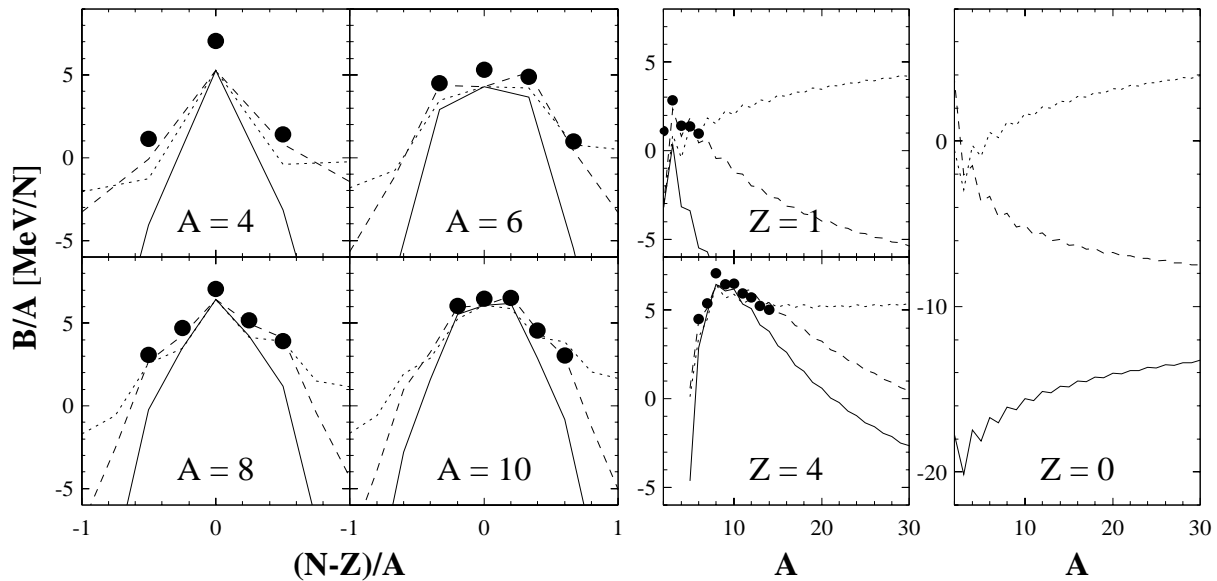


Figure 30: Binding energy per nucleon for different isobars (left), H and Be isotopes (middle), and multinucleons (right). The symbols are experimental data; the lines are results of the liquid drop formula [Eq. (1)] with different asymmetry terms: standard (solid), surface corrected (dashed), and one derived from a neutron-skin density (dotted, see text).

one fitted on heavier nuclei —, it is clear that the asymmetry effect is overestimated.

Some versions of the liquid drop formula have included surface effects in the calculation of  $a_a$ : the effect of the asymmetry energy decreases for increasing surface-to-volume ratio (lighter nuclei) [5, p. 197]. These liquid drop formulae<sup>‡</sup> provide a much better description of very asymmetric light nuclei (Fig. 30, dashed lines). The differences are moderate for known nuclei; for multinucleons, however, they may rise up to 20 MeV/N!

One hypothesis in the derivation of the asymmetry term within the Fermi gas model is that neutrons and protons move within the *same* volume. When the system becomes very neutron-rich we know that this may not be the case. This effect can be estimated in a simple way by considering a Fermi gas in which the density is  $\rho_0$  all over the nucleus but with two phases: a central core with  $N = Z$  and the extra neutrons outside the core forming a neutron skin. The resulting asymmetry term is also linear with  $A$  for multinucleons, but the  $a_a$  parameter needed in order to describe known nuclei is much smaller,  $\sim 6$  MeV (Fig. 30, dotted lines).

The latter is a too simple approximation, not only because of the density assumed but also because

only the kinetic contribution to the asymmetry energy is estimated in the Fermi gas model [2, p. 241]. But Fig. 30 displays clearly **how far** multinucleons are from nuclei we know: calculations that describe known nuclei within few MeV/N may diverge up to 20 MeV/N when a proton-free system is considered...

### Ab initio calculations

These are the QMC calculations that were described in Sec. 2.3. They also predict that multinucleons should not exist. They are much more formal than the macroscopic liquid drop model, and are considered as an exact microscopic approach of the many-nucleon problem [12, 35, 38]. The results, however, are quantitatively similar (Figs. 15,30) as both reproduce binding energies at the few MeV level.

In the quantitative level, the key ingredient of QMC is the three-body force, without which the results are off the data by about 10 MeV (Fig. 15). Unfortunately, this is the less *ab initio* input of the model. The parameters of  $V_{NNN}$  are fitted in order to reproduce the known nuclei, and therefore the agreement with data is not so surprising. Neither is the lack of predicting power.

For example, the first versions fitted on  ${}^4\text{He}$  “predicted” a decrease of binding energy with increasing

<sup>‡</sup>For a recent one see [67].

isospin [68] —  ${}^4,6,8\text{He}$  are  $T = 0, 1, 2$ , respectively. The data showed the opposite trend. New forces were then fitted to the  $T \neq 0$  isotopes in order to reproduce the right trend. Note that  $A \geq 4$   $n$  systems are  $T \geq 2$ , the isospin values for which the interactions are less known.

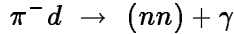
### The neutron-neutron interaction

The accurate  $V_{NN}$  potentials used in the QMC model are fitted to the  $n$ - $p$  and  $p$ - $p$  scattering data base. The  $n$ - $n$  interaction cannot be fitted as no  $n$ - $n$  scattering data exist. The  $N$ - $N$  scattering is parametrized in terms of the phase shift  $\delta$  which, at low energy  $k$ , can be expanded as:

$$k \cot \delta = \frac{-1}{a_{NN}} + \frac{1}{2} r_{NN} k^2 + \mathcal{O}(k^4) \equiv \frac{-1}{a(k)} \quad (40)$$

The two parameters defining the interaction at low energy are  $r_{NN}$ , the *effective range*, and  $a_{NN}$ , the *scattering length*, which corresponds to  $a(0)$  and dominates thus the interaction at very low energies [5, p. 68]. The parametrization in Eq. (40) is introduced as, at low energy, the cross-section can be written as  $\sigma_{NN}(k) = 4\pi a(k)^2$ .

Experimentally,  $a_{nn}$  can be determined from reactions in which the final state consists of two neutrons not perturbed by other particles. The best candidate is [20, 69, 70]:



which is shown in Fig. 7. The reaction  $\mu^- d \rightarrow (nn) + \nu_\mu$  has not been measured yet, and the values extracted from  $nd \rightarrow (nn) + p$  have been shown to depend on the theoretical treatment of three-nucleon forces in the final state [1].

The accepted value is  $a_{nn} = -18.5 \pm 0.4$  fm [1]. It is less accurate than the well-known  $a_{np}$  and  $a_{pp}$  and, moreover, represents just the scattering parameter at zero energy for the  ${}^1S_0$   $n$ - $n$  interaction:  $a^S(0)$ . In QMC calculations, however, we need to know  $a^L(k)$ . Therefore, charge independence (CI) of the  $N$ - $N$  interaction has to be assumed: the  $n$ - $n$  interaction evolves with energy and angular momentum as the  $n$ - $p$  and  $p$ - $p$  interactions do. We know, however, that already the  $n$ - $p$  and  $\pi^0$ - $\pi^\pm$  mass differences *must* break CI [1]. Only recently terms that break CI have been added to the interactions [12].

**Note:** the  $n$ - $n$  interaction used in the different models is thus purely theoretical, *it has never been measured*. Measuring this interaction remains a huge experimental challenge.

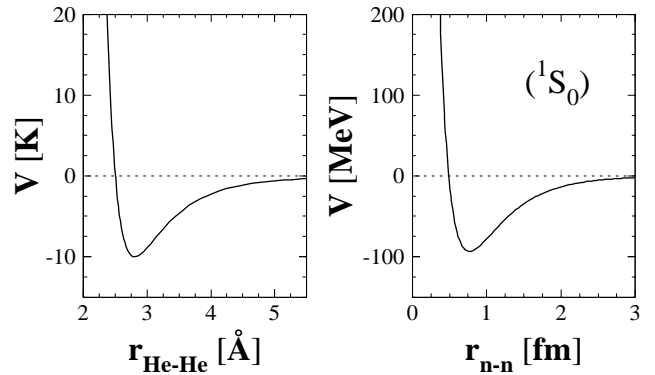


Figure 31: Comparison between the  ${}^3\text{He}$  interatomic potential and the  $n$ - $n$  potential in the singlet state.

### Some clues for

We have seen that the arguments against multineutrons are only moderately strong. Are there arguments for their existence?

The fact that two neutrons do not form a bound system and that neutrons are fermions is used as an argument against the existence of multineutrons. But there is an analog problem in atomic physics: **liquid ( ${}^3\text{He}$ ) $_N$  drops**. Indeed,  ${}^3\text{He}$  atoms are also fermions and their interaction, although attractive, is also too weak to form a dimer. Since a very high number of atoms form a liquid drop, theoretical studies have been undertaken to find the critical number of atoms needed to form a bound system, leading to  $N \sim 30$  [71].

Could it be that a critical number exists also for neutron drops? The interaction potentials, although at very different scales, have indeed a similar shape (Fig. 31). The same type of calculations [71] are, however, not yet available at the nuclear level, as the  $n$ - $n$  potential is much more complex than just the central part drawn in Fig. 31. Work in this direction is in progress [68].

Another hint can be extracted from the known light, **neutron-rich masses**. Besides the odd-even staggering, the overall trend for all the elements is that the binding energy decreases monotonically as more and more neutrons are added (Fig. 1). There are, however, two exceptions to this rule: hydrogen and helium [Fig. 32(a)]. It is intriguing that this neutron binding effect appears only for nuclei with *very few protons*, and that the maximum effect seems to be associated to *four neutrons*:  $\alpha + 4n$  leads to the particularly stable  ${}^8\text{He}$ , and  ${}^5\text{He} + 4n$  leads to an almost bound  ${}^9\text{He}$ .



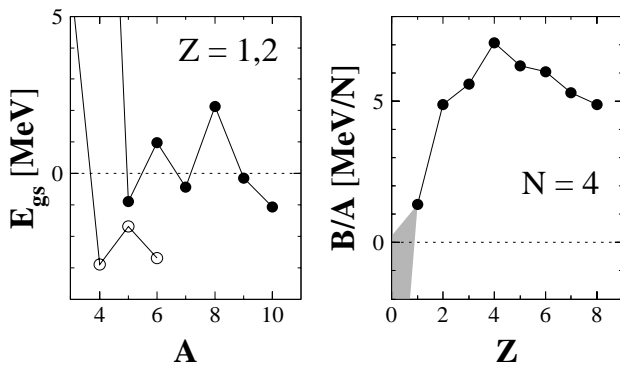


Figure 32: Nuclear mass systematics [44, 72, 73]: (a) binding energy with respect to the first particle threshold for H and He isotopes; (b) binding energy per nucleon for  $N = 4$  isotones.

The binding energy per nucleon for light  $N = 4$  isotones [Fig. 32(b)] has been recently extended down to  $Z = 1$  [44]. The sequence  ${}^8\text{Be}$ - ${}^7\text{Li}$ - ${}^6\text{He}$ - ${}^5\text{H}$  follows a decrease modulated by the  $\pm\delta$  pairing term [Eq. (1)]. The next member of the sequence,  ${}^4\text{n}$ , should continue the decrease but with a  $+\delta$  contribution. Therefore, there might be still room for a positive binding energy.

**Note:** the fact that the neighbouring  ${}^{4,5}\text{H}$  are not particle stable would not be in contradiction with particle stability of  ${}^4\text{n}$ . These hydrogen isotopes have a positive binding energy of about 6 MeV, but they are unbound only because  ${}^3\text{H}$  is bound by 7.7 MeV, and thus they decay into a triton and 1,2 neutrons. But in the case of  ${}^4\text{n}$  there are no bound subsystems, and then even a 1 keV binding energy would lead to a bound tetra-neutron.

## 4.2 The quest: 1960s-2000s

Experimentally, despite the efforts made in the past forty years, no limit has yet been placed on the binding energy of  ${}^4\text{n}$  — or any other  ${}^A\text{n}$ . Rather only limits on the production cross-sections could be estimated from two-step or direct reactions.

### Two-steps reactions

The principle consists of the production of  ${}^4\text{n}$  in reactions such as neutron-induced fission of U [74, 75] or proton and light-ion fragmentation of a heavy target [76, 77]. Any recoiling  ${}^A\text{n}$  could be then signaled by the radiochemical separation of decay products from  $({}^A\text{n}, xn)$  reactions in a secondary target. An extremely pure target and a detailed analysis of all pos-

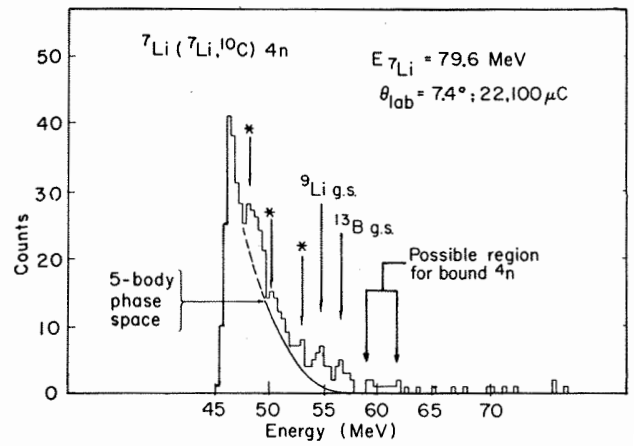


Figure 33: Energy spectrum of  ${}^{10}\text{C}$  from the reaction  ${}^7\text{Li}({}^7\text{Li}, {}^{10}\text{C})4n$ . Known contaminant reactions are indicated either explicitly or by an asterisk [83].

sible backgrounds are thus needed. As such only upper limits for the  ${}^4\text{n}$  production cross-section, assuming cross-sections for the  $({}^A\text{n}, xn)$  reactions, could be determined. The only positive claim [76] was later explained as arising from an underestimation of the production of very energetic tritons [77].

### $\pi^-$ charge exchange

A step forward was given with double pion charge exchange ( $\text{D}\pi\text{CX}$ ) reactions on helium:  ${}^A\text{He}(\pi^-, \pi^+)An$ . By detecting the  $\pi^+$ , states in the  $An$  system could be signaled by discrete values of the pion energy. The technique has been applied to  ${}^3,4\text{He}$  in order to study  ${}^3,4\text{n}$  [78, 79, 80]. The different  $\pi^+$  spectra, once the backgrounds subtracted, have shown no significant evidence for bound or resonant states. The cross-section — one pion has to change the charge of two protons — is very low, typically tens of nb [80].

This reaction was already tried inside a lead nucleus:  ${}^{208}\text{Pb}(\pi^-, \pi^+){}^4\text{n}$ . The idea was to induce then a second reaction in the thick target in which the tetra-neutron would be absorbed into  ${}^{212}\text{Pb}$  [81]. No  $\alpha$  decay energies corresponding to  ${}^{212}\text{Pb}$  were observed. Another variant of this technique was single pion charge exchange:  ${}^3\text{H}(\pi^-, \gamma)3n$ , but the photon energy showed no evidence for a trineutron state [82].

### Multinucleon transfer

The two-body kinematics idea of  $\text{D}\pi\text{CX}$  was applied to heavy-ion transfer reactions of the type  $a(b, c)An$ ,

without success [83, 84, 85, 86]. The cross-section was still very low, and the use of stable beam-target combinations limited the search to  ${}^3,4\text{n}$ . There are, in addition, other problems that are clear in Fig. 33: (i) the background inherent to missing mass techniques due to target impurities — arrows and counts in the unphysical region beyond 62 MeV; (ii) the precise knowledge of the  $(A + 1)$  phase space, on top of which the signal should appear; and (iii) the bias introduced by the fact that both the  ${}^A\text{n}$  and the ejectile have to be formed in the reaction.

### 4.3 A new approach

All the experiments reviewed have in common that: (i) they relied on extremely low cross-sections; (ii) the multineutron signal was not expected in a background-free region (see Fig. 33); and (iii) they used stable (or almost) beams and targets. Also that none lead to a positive result. Does the availability of neutron-rich beams provide new possibilities in this field?

#### Principle

We have discussed in the two preceding sections clustering phenomena in light, neutron-rich nuclei. If multineutrons *do exist* one should consider them as any other cluster, and thus expect that a (more or less) significant component of the wave function of these nuclei could correspond to a multineutron configuration.

Therefore they should be liberated in breakup reactions, in which relatively high cross-sections are encountered (Sec. 2). Moreover, the detection of neutrons in coincidence with the reaction  $({}^A\text{X}, {}^{A-xn}\text{X})$  provides a clean selection of the reaction channel. But how can we distinguish between the production of  $xn$  and  ${}^x\text{n}$ ?

The principle is similar to that used by Chadwick 70 years ago for the discovery of the neutron: infer the mass of the neutral particle by the recoil energy of a proton [88]. Indeed, the predominant mechanism for the detection of neutrons in a liquid scintillator, such as that used in DEMON (Fig. 8), is  $n$ - $p$  scattering [89], in which the proton recoils with an energy ( $E_p$ ) up to that of the incident neutron. In general, the neutron does not lose all its energy in the interaction and may escape from the detector [22].

The energy of the proton may then be compared to the energy per nucleon of the incident particle derived from the time-of-flight ( $E_n$ ). For a single neutron and an ideal detector  $E_p/E_n \leq 1$ , but in the

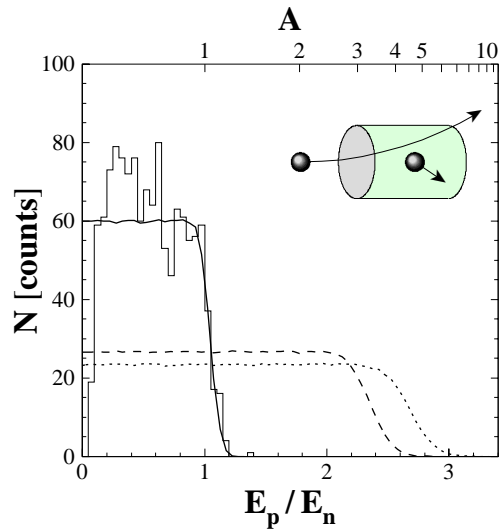


Figure 34: Distribution of the ratio of proton energy,  $E_p$  (MeV), to the energy derived from the flight time,  $E_n$  (MeV/N), for data from the reaction  $({}^{14}\text{Be}, {}^{12}\text{Be}+n)$  and for simulations of elastic scattering of  ${}^1,3,4\text{n}$  (solid, dashed and dotted lines, respectively) on protons [87].

case of a multineutron  $E_p$  can exceed the incident energy *per nucleon* and  $E_p/E_n$  may take on a range of values extending beyond 1 ( $\sim 1.4$  due to finite resolutions of DEMON), as shown in Fig. 34. The  ${}^x\text{n}$  signal is thus expected in a region **well separated** from the  $xn$  background.

#### Test on data

The technique was tested [87] on existing data from the breakup of  ${}^{14}\text{Be}$  (Sec. 2). This system, together with  ${}^8\text{He}$ , is a promising candidate as protons can be considered to be “confined” inside  $\alpha$  particles and the  $4n$  thresholds are the lowest known ( $S_{4n} = 3.1$  MeV for  ${}^8\text{He}$  and 5.0 for  ${}^{14}\text{Be}$ ). The detection of neutrons produced in the reaction  $({}^{14}\text{Be}, {}^{12}\text{Be}+n)$  is displayed in Fig. 34; a channel in which multineutrons should be absent. We observe that the flat distribution predicted for  $n$ - $p$  scattering describes the data well.

The charged fragments produced in the breakup of the beam particles were identified using the energy loss ( $\Delta E_{\text{Si}}$ ) and residual energy ( $E_{\text{CSi}}$ ) signals derived from the telescope (Fig. 8). One dimensional spectra representing the particle identification (PID) were constructed projecting along the hyperbolas corresponding to Be isotopes [90, 91]. The PID distribution (left panel in Fig. 35) exhibits peaks corresponding to isotopes of H, He, Li and Be, in which  ${}^{10,12}\text{Be}$  are well resolved (the two higher-lying peaks).

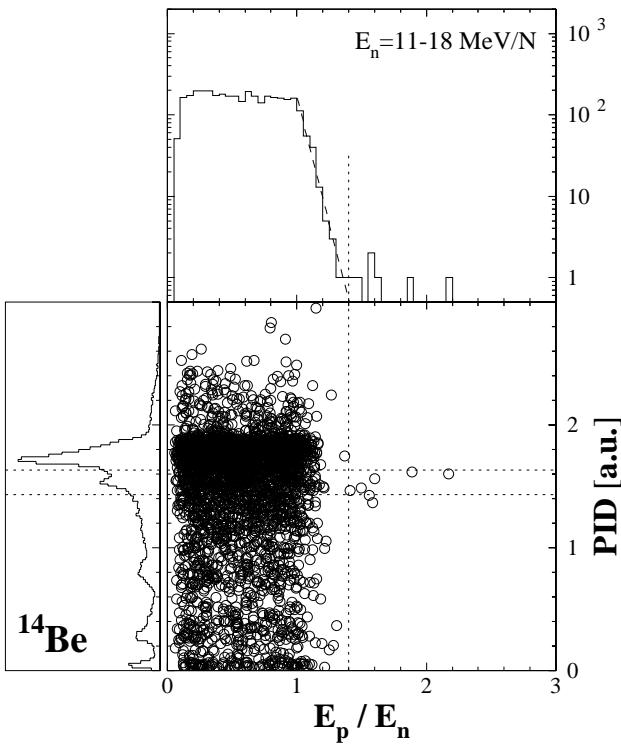


Figure 35: Scatter plot, and the projections onto both axes, of the particle identification parameter PID vs  $E_p/E_n$  for the data from the reaction ( $^{14}\text{Be}$ ,  $X+n$ ). The dotted lines correspond to  $E_p/E_n = 1.4$  and to the region centred on the  $^{10}\text{Be}$  peak [87].

The  $E_p/E_n$  distribution (upper panel in Fig. 35) exhibits a plateau up to 1 followed by a sharp decline up to 1.4, which may be fitted to an exponential distribution (dashed line). In the region where  $^4\text{n}$  events may be expected to appear,  $E_p/E_n > 1.4$ , six events ranging from 1.4 to 2.2 are observed. All of them fall within a region centred on  $^{10}\text{Be}$ . No such events were observed for two other components present in the beam,  $^{11}\text{Li}$  and  $^{15}\text{B}$  [87].

Several potential sources of events with  $E_p/E_n > 1.4$  not involving the formation of a multineutron have been considered [87], but none was found to account for the fact that the six events appear to be produced in association with  $^{10}\text{Be}$  fragments (17% of the total yield) while no events appear in association with other fragments with comparable (H-He-Li, 19%) or higher ( $^{12}\text{Be}$ , 47%) yields. Therefore, the six events exhibit the characteristics of a multineutron liberated in the breakup of  $^{14}\text{Be}$ , most probably in the channel  $^{10}\text{Be}+^4\text{n}$ .

#### 4.4 The near future

The limited statistics, however, together with experimental constraints due to the fact that this experiment was not planned for multineutron detection [87], require much caution until these results are confirmed. At least as much as Chadwick expressed in 1932: “*the difficulties [to explain the results] disappear, however, if it be assumed that the radiation consists of particles of mass 1 and charge 0, or neutrons*” ...

#### Dedicated experiments in progress

At the time of writing this document, three dedicated experiments have just been undertaken at GANIL:

- $\alpha$ -particle transfer from a  $^8\text{He}$  beam to a deuterium target, leading to a  $^6\text{Li}+4\text{n}$  final state [3, E. Rich]. The energy of  $^6\text{Li}$  should exhibit peaks associated to  $4\text{n}$  states (as in Fig. 33).
- $^8\text{He}$  breakup into  $^4\text{He}+4\text{n}$  [92]. The high intensity delivered by SPIRAL,  $1.5 \cdot 10^4$  pps, should lead to a clearer signal *if* a tetra-neutron configuration is significantly present in  $^8\text{He}$  — the four valence neutrons are in  $p$  orbits, whereas in  $^4\text{n}$  they should be in  $s$  and  $p$  orbits.
- $^{14}\text{Be}$  breakup into  $^{10}\text{Be}+4\text{n}$  [93]. A new array of 16 CsI crystals from the CHARISSA collaboration should, in addition, extend the study to the  $^8\text{Be}+6\text{n}$  channel through the detection of the two  $\alpha$  particles.

The beam was only partly available for the two breakup experiments. However, the analysis of the three data sets may shed light on the debate in the coming months.

Concerning new candidate nuclei, the measurement of the mass of  $^{19}\text{B}$  should be undertaken. Using the extrapolated value in [72], this nucleus would exhibit the lowest  $S_{4\text{n}}$  value known, only 2 MeV, and thus the probability of finding a  $^4\text{n}$  configuration should be higher than in  $^{14}\text{Be}$  (5 MeV) or  $^8\text{He}$  (3.1 MeV). A question that should have to be considered in parallel is the development of alternative experimental programs on the measurement of the  $n$ - $n$  interaction.

#### Theoretical calculations

These results have triggered the attention of many theoretical groups. To date, all the calculations suggest the need of many-body forces in order to bind

light multineutrons — a recent example of a calculation using two-body forces can be found in [94].

More complete calculations are being developed addressing, either the existence of multineutrons itself, either the changes that need to be introduced in the present interactions in order to bind them. These efforts may also lead to a deeper exploration of the  $n$ - $n$  interaction, very often treated in a rather simple way, and of many-body forces.

## Neutron stars

One could argue that multineutrons, bound systems of neutrons, already exist: neutron stars. They are, however, at a very different size scale and held together by gravity. Is there any straightforward link between the possible existence of multineutrons at the nuclear scale and the characteristics of neutron stars?

The easiest approach consists in adding the gravitational term to Eq. (1) and calculating the minimum number of neutrons needed to hold the system [95, p. 226]. The result is of course fully dependent on the asymmetry term. For the solid and dashed lines in Fig. 30 the values are  $A_{\min} \sim 4 \cdot 10^{55}$  and  $10^{57}$ ,  $R \sim 3.4$  and  $10$  km, and  $M/M_{\odot} \sim 0.04$  and  $1$ , respectively. The surface corrected term gives the right orders of magnitude, although the density when using Eq. (1) is assumed to be  $\rho_0$  — due to gravity it should be higher — and we have ignored how  $10^{57}$  neutrons could get together.

After a supernova explosion, the burnt out center of the star, mostly iron of  $1$ – $2 M_{\odot}$ , collapses under the gravitational force. The Fermi energy of electrons increases and the  $p + e^{-} \rightarrow n + \nu_e$  capture process begins, while the inverse ( $\beta$  decay) gets blocked by the Pauli principle — the electron gas is degenerate and there are no vacant states for the emitted electron. Nuclei become very neutron-rich and, in the end, they lose their identity and the interior of the star is mostly composed of neutrons, whose Fermi pressure stops the implosion. For heavier masses, the implosion goes on and the star ends up as a black hole.

The  ${}^{56}\text{Fe} \rightarrow 56n$  collapse can be described within the Fermi gas model [2, p. 244]. Minimizing the energy of the neutron gas with respect to the radius leads, for  $M/M_{\odot} = 1.5$ , to  $R = 12$  km and  $\rho = 1.5\rho_0$ . The interior density, however, can reach even much higher values, and a complete description of how neutron matter behaves at such high densities is not yet available [96, p. 598]. In the core of the

star one could find hyperons, pions, or even deconfined quarks. A strong debate is nowadays open.

The possible existence of multineutrons would not have any implication in the core composition, not even in the whole interior as at densities beyond  $\rho_0$  nuclei dissolve — also neutral nuclei would. They could only appear in the inner crust, in which  ${}^{56}\text{Fe}$  coexists with very neutron-rich nuclei and free neutrons, but this is a very small part of the star and any effect would be far beyond the present experimental capabilities.

On the other hand, attempts are being made in order to link the properties of neutron stars with those of the most neutron-rich stable nucleus,  ${}^{208}\text{Pb}$  [97]. Theoretical models explore in this way the  $N$ - $N$  interaction for  $N > Z$  [98]. In that sense, multineutrons could provide a very important input, as their possible existence would constraint strongly the  $N$ - $N$  interaction in an almost proton-free environment like the one found in neutron stars.

## 5 Summary

Among the extended landscape of exotic nuclei, we have reviewed three different kinds for which most of the well established nuclear properties break down. In all three, clustering of nucleons and correlations between clusters become the relevant degrees of freedom, instead of the behaviour of the  $A$  nucleon system as a whole.

Besides the understanding of cluster correlations, many-neutron **halo nuclei** provide for the first time very dilute nuclear matter in its ground state. This is a unique frame in which the  $N$ - $N$  interaction can be studied. These systems represent also an almost experimental input to three-body forces, which play an increasing role in theoretical descriptions of light nuclei and for which no direct experimental data exist. These systems are right on the drip line, and give rise to many — still unanswered — questions. How do correlations survive across the drip line? May they be able to bind systems far beyond? Is the number of halo neutrons limited?

Concerning **nuclear molecules**, it was surprising that, despite the huge differences between the atomic and nuclear cases, the molecular orbitals are almost equivalent in both. With the simple deformed harmonic oscillator model, we have seen how deformation of the nucleus can be responsible for the clustering effects observed through the nodes appearing in the wave functions. Complex dimers are being studied both theoretical and experimentally, but the

studies of trimers, based for example in the  $3\alpha$  chain of carbon, are just starting.

The third kind was the most exotic of them: **neutron clusters**. So exotic that its existence has not been confirmed yet. Intuition, and a long list of challenging experiments and conventional calculations, tell us that they should not exist. But intuition and calculations are not enough. Very neutron-rich beams open a new way in this field, and any result — confirmation or not of the first hints observed — will have important implications in the understanding of the  $n$ - $n$  force.

## Acknowledgements

This lecture was not ment to be an extensive review article of haloes, molecules and multineutrons, but just a guide to the student through some selected aspects of these three fields. Most of the experimental results I have used to that end are the result of the common effort of the collaborations listed in [16, 62, 87], and in particular the DEMON and CHARISSA crews.

This document would not have been possible without the discussions and help I received from my colleagues Nigel Orr (haloes and multineutrons), Martin Freer and Wilton Catford (molecules), Marc Labiche, Emmanuel Sauvan, Jean-Luc Lecouey and Guillaume Normand (analysis of the huge amount of data), and Denis Lacroix (nuclear models). The support provided by the staffs of LPC (in particular Jean-Marc Gautier, Philippe Desrues, Jean-Marc Fontbonne, Laurent Hay, David Etasse and Joël Tilletier) and GANIL in preparing and executing the experiments is gratefully acknowledged.

## Problèmes

Pour ceux qui ont suivi le cours :

1. Retrouver et tracer les fonctions d'onde associées à un potentiel de puits carré (Fig. 4). Modifier son rayon et/ou sa profondeur pour voir le processus d'étalement de la probabilité de présence à l'extérieur du puits.
2. Calculer l'énergie du photon associé au processus de capture ( $p, \gamma$ ) sur les différents constituants d'un faisceau d' ${}^6\text{He}$  à 40 MeV/N (Fig. 6).
3. Étudier la cinématique de la réaction  $\pi^- d \rightarrow nn\gamma$  (Fig. 7) en considérant que la capture du

neutron se produit au repos. Quelles sont les énergies maximales/minimales du photon et des neutrons?

4. Calculer la distance rms entre deux nucléons dans une sphère de rayon  $r_0 A^{1/3}$  (Fig. 10) et la comparer à celle obtenue à partir d'une distribution Gaussienne équivalente ( $\sigma = \sqrt{3/5} r_0 A^{1/3}$ ).
5. Tracer les orbitales moléculaires de la Fig. 20 à partir des orbitales atomiques dans l'atome d'hydrogène pour plusieurs distances interatomiques.
6. Tracer les orbitales de l'oscillateur harmonique déformé pour  $w_t/w_z = 2$  et 3 (Figs. 24-26).
7. Dériver l'énergie d'asymétrie selon le modèle du gaz de Fermi pour un noyau à densité constante mais avec un cœur central  $N = Z$  plus les neutrons additionnels à l'extérieur (Fig. 30).
8. Calculer l'énergie de recul maximale du proton dans la diffusion élastique  ${}^A n-p$  (Fig. 34).
9. Calculer le nombre de neutrons minimal requis pour qu'un multineutron soit lié en rajoutant le terme gravitationnel à la formule de goutte liquide standard [Eq. (1)].

## References

- [1] R. Machleidt, Nucl. Phys. **A689**, 11c (2001); R. Machleidt, I. Slaus, J. Phys. G **27**, R69 (2001).
- [2] B. Povh *et al.*, "Particles and Nuclei: and Introduction to the Physical Concepts", Springer (1999).
- [3] This book.
- [4] M.V. Zhukov *et al.*, Phys. Rep. **231**, 151 (1993).
- [5] W.F. Hornyak, "Nuclear Structure", Academic Press (1975).
- [6] I. Tanihata *et al.*, Phys. Rev. Lett. **55**, 2676 (1985); Phys. Lett. B **206**, 592 (1988).
- [7] P.G. Hansen, B. Jonson, Europhys. Lett. **4**, 409 (1987).
- [8] E. Arnold *et al.*, Phys. Lett. B **197**, 311 (1987).
- [9] B. Blank *et al.*, Z. Phys. A **343**, 375 (1992).
- [10] J.S. Al-Khalili, J.A. Tostevin, Phys. Rev. Lett. **76**, 3903 (1996); J.S. Al-Khalili, J.A. Tostevin, I.J. Thompson, Phys. Rev. C **54**, 1843 (1996).
- [11] N.A. Orr *et al.*, Phys. Rev. Lett. **69**, 2050 (1992); N.A. Orr, Nucl. Phys. **A616**, 155c (1997) and references therein.

- [12] S.C. Pieper, Eur. Phys. J. A **13**, 75 (2002).
- [13] Y.T. Oganessian, V.I. Zagrebaev, J.S. Vaagen, Phys. Rev. Lett. **82**, 4996 (1999).
- [14] I.V. Krouglov, M. Avrigeanu, W. von Oertzen, Eur. Phys. J. A **12**, 399 (2001).
- [15] M. Hoefman *et al.*, Phys. Rev. Lett. **85**, 1404 (2000).
- [16] E. Sauvan *et al.*, Phys. Rev. Lett. **87**, 042501 (2001).
- [17] K. Arai, Y. Suzuki, K. Varga, Phys. Rev. C **51**, 2488 (1995).
- [18] K. Arai, Y. Suzuki, R.G. Lovas, Phys. Rev. C **59**, 1432 (1999).
- [19] M. Nikolić, “Kinematics and Multiparticle Systems”, Gordon and Breach, New York (1968), p. 33.
- [20] M.A. Preston, R.K. Bhaduri, “Structure of the Nucleus”, Addison-Wesley (1975), p. 45.
- [21] F.M. Marqués *et al.*, Phys. Lett. B **476**, 219 (2000).
- [22] F.M. Marqués *et al.*, Nucl. Instr. Meth. A **450**, 109 (2000).
- [23] W.A. Zajc *et al.*, Phys. Rev. C **29**, 2173 (1984).
- [24] G.I. Kopylov, Phys. Lett. B **50**, 472 (1974).
- [25] R. Lednicky, L. Lyuboshits, Sov. J. Nucl. Phys. **35**, 770 (1982).
- [26] F.M. Marqués *et al.*, in preparation.
- [27] F.M. Marqués *et al.*, Phys. Rev. C **64**, 061301 (2001).
- [28] D.H. Perkins, “Introduction to High Energy Physics”, Addison-Wesley (1987), p. 122.
- [29] N. Vinh Mau, J.C. Pacheco, Nucl. Phys. **A607**, 163 (1996).
- [30] D. Baye, Nucl. Phys. **A627**, 305 (1997).
- [31] P.G. Hansen, A.S. Jensen, B. Jonson, Ann. Rev. Nucl. Part. Sci. **45**, 591 (1995).
- [32] N.B. Shul’gina *et al.*, Phys. Rev. C **62**, 014312 (2000).
- [33] P. Descouvemont, A. Kharbach, Phys. Rev. C **63**, 027001 (2001).
- [34] P. Descouvemont, Phys. Rev. C **52**, 704 (1995).
- [35] R.B. Wiringa, S.C. Pieper, Phys. Rev. Lett. **89**, 182501 (2002).
- [36] Y. Kanada-En’yo, H. Horiuchi, A. Doté, Phys. Rev. C **60**, 064304 (1999).
- [37] P. Descouvemont, private communication.
- [38] R.B. Wiringa *et al.*, Phys. Rev. C **62**, 014001 (2000).
- [39] A.V. Belozorov *et al.*, Nucl. Phys. **A636**, 419 (1998).
- [40] J.L. Lecouey, PhD Thesis, Université de Caen (2002), LPCC T 02-03.
- [41] G. Normand *et al.*, in preparation.
- [42] L.V. Chulkov, G. Schrieder, Z. Phys. A **359**, 231 (1997).
- [43] C. Forssén, B. Jonson, M.V. Zhukov, Nucl. Phys. **A673**, 143 (2000).
- [44] A.A. Korshennikov *et al.*, Phys. Rev. Lett. **87**, 092501 (2001).
- [45] W. von Oertzen *et al.*, Nucl. Phys. **A588**, 129c (1995).
- [46] A.A. Korshennikov *et al.*, Phys. Lett. B **326**, 31 (1994).
- [47] Y. Iwata *et al.*, Phys. Rev. C **62**, 064311 (2000).
- [48] M. Meister *et al.*, Nucl. Phys. **A700**, 3 (2002).
- [49] A.S. Jensen, K. Riisager, Phys. Lett. B **264**, 238 (1991).
- [50] E. Almqvist, D.A. Bromley, J.A. Kuehner, Phys. Rev. Lett. **4**, 515 (1960).
- [51] M. Freer, A.C. Merchant, J. Phys. G **23**, 261 (1997).
- [52] W. von Oertzen, Z. Phys. A **354**, 37 (1996).
- [53] W. von Oertzen, Z. Phys. A **357**, 355 (1997).
- [54] M.W. Hanna, “Quantum Mechanics in Chemistry”, W.A. Benjamin Inc. (1965).
- [55] J.M. Eisenberg, W. Greiner, “Nuclear Theory 1”, North Holland, Amsterdam (1975).
- [56] P. Holzer, U. Mosel, W. Greiner, Nucl. Phys. **A138**, 241 (1969).
- [57] B. Imanishi, W. von Oertzen, Phys. Rep. **155**, 29 (1987).
- [58] W. von Oertzen, Eur. Phys. J. A **11**, 403 (2001).
- [59] M. Freer, Nucl. Phys. **A685**, 146c (2001).
- [60] N. de Takacsy, Nucl. Phys. **A178**, 469 (1972).
- [61] H.G. Bohlen *et al.*, Nuovo Cimento **111**, 841 (1998).
- [62] M. Freer *et al.*, Phys. Rev. Lett. **82**, 1383 (1999).
- [63] P.J. Leask *et al.*, J. Phys. G **27**, B9 (2001).
- [64] A. Saito *et al.*, submitted to World Scientific.
- [65] A.A. Ogloblin, Y.E. Penionzhkevich, “Treatise on Heavy-Ion Science (vol. 8): Nuclei Far From Stability”, Ed. D.A. Bromley, Plenum Press, New York (1989), p. 261 and references therein.
- [66] D.R. Tilley, H.R. Weller, G.M. Hale, Nucl. Phys. **A541**, 1 (1992) and references therein.
- [67] P. Danielewicz, nucl-th/0301050.
- [68] J. Carbonell, private communication.
- [69] O. Schori *et al.*, Phys. Rev. C **35**, 2252 (1987).
- [70] C.R. Howell *et al.*, Phys. Lett. B **444**, 252 (1998).

- [71] M. Barranco, J. Navarro, A. Poves, Phys. Rev. Lett. **78**, 4729 (1997); R. Guardiola, J. Navarro, Phys. Rev. Lett. **84**, 1144 (2000).
- [72] G. Audi, A.H. Wapstra, Nucl. Phys. **A565**, 1 (1993).
- [73] L. Chen *et al.*, Phys. Lett. B **505**, 21 (2001).
- [74] J.P. Schiffer, R. Vandenbosch, Phys. Lett. **5**, 292 (1963).
- [75] S. Cierjacks *et al.*, Phys. Rev. **137**, B345 (1965).
- [76] C. Détraz, Phys. Lett. **66B**, 333 (1997).
- [77] F.W.N. de Boer *et al.*, Nucl. Phys. **A350**, 149 (1980).
- [78] J.E. Ungar *et al.*, Phys. Lett. **144B**, 333 (1984).
- [79] T.P. Gorringer *et al.*, Phys. Rev. C **40**, 2390 (1989).
- [80] J. Gräter *et al.*, Eur. Phys. J. A **4**, 5 (1999).
- [81] D. Chultem *et al.*, Nucl. Phys. **A316**, 290 (1979).
- [82] J.P. Miller *et al.*, Nucl. Phys. **A343**, 347 (1980).
- [83] J. Cerny *et al.*, Phys. Lett. **53B**, 247 (1974).
- [84] G.G. Ohlsen, R.H. Stokes, P.G. Young, Phys. Rev. **176**, 1163 (1968).
- [85] A.V. Belozyorov *et al.*, Nucl. Phys. **A477**, 131 (1988).
- [86] H.G. Bohlen *et al.*, Nucl. Phys. **A583**, 775 (1995).
- [87] F.M. Marqués *et al.*, Phys. Rev. C **65**, 044006 (2002).
- [88] J. Chadwick, Nature **129**, 312 (1932).
- [89] J. Wang *et al.*, Nucl. Instr. Meth. A **397**, 380 (1997).
- [90] M. Labiche, PhD Thesis, Université de Caen (1999), LPCC T 99-03.
- [91] K. Riisager *et al.*, Nucl. Phys. **A540**, 365 (1992).
- [92] F.M. Marqués *et al.*, GANIL proposal E415 (2001).
- [93] F.M. Marqués *et al.*, GANIL proposal E378 (2000).
- [94] C.A. Bertulani, V. Zelevinsky, nucl-th/0212060.
- [95] K. Heyde, “Basic Ideas and Concepts in Nuclear Physics”, IOP Publishing Ltd (1999).
- [96] B.W. Carroll, D.A. Ostlie, “An Introduction to Modern Astrophysics”, Addison-Wesley (1996).
- [97] C. Horowitz, J. Piekarewicz, Phys. Rev. Lett. **86**, 5647 (2001).
- [98] S. Schramm, nucl-th/0210053.